Bulletin of Volcanology (2025) 87:10
https://doi.org/10.1007/s00445-025-01794-4

RESEARCH ARTICLE

Probabilistic tephra fallout hazard maps for Sangay volcano, Ecuador

Alessandro Tadini[1,2] · Federica Pardini[1] · Andrea Bevilacqua[1] · Benjamin Bernard[3] · Pablo Samaniego[2] · Mattia de' Michieli Vitturi[1] · Alvaro Aravena[1,4,5] · Silvana Hidalgo[3] · Olivier Roche[2] · Nourddine Azzaoui[6] · Augusto Neri[1] · Jorge Aguilar[3]

Received: 13 July 2024 / Accepted: 8 December 2024 / Published online: 29 January 2025

Abstract
Sangay volcano (Ecuador) shows a quasi-continuous activity at least since the seventeenth century and has produced several eruptions which affected towns and cities at considerable distance (up to > 170 km). For this reason, despite its remote location, recent efforts were aimed at reviewing its volcanic history, quantifying the occurrence probability of four eruptive scenarios of different magnitude (Strong Ash Venting, Violent Strombolian, sub-Plinian, and Plinian) and the associated uncertainty, and, for each eruptive scenario, estimating the probability distribution of key eruptive source parameters (fallout volume, average plume height, and eruption duration). In this study, we utilize such information to produce probabilistic hazard maps and curves. To this aim, we use coupled plume and dispersal models (PLUME-MOM-TSM and HYSPLIT, respectively) with the application of a novel workflow for running an ensemble of thousands of simulations following a stochastic sampling of input parameters. We produced probabilistic hazard maps for each scenario by considering four ground load thresholds (i.e., 0.1, 1, 10, and 100 kg/m^2) and two types of model initialization strategies, based on the elicited total deposit volume and on the elicited plume height, respectively, which produced non-negligible differences. In addition, we produced hazard curves for nine sites of interest from a risk perspective, corresponding to towns/cities potentially affected by tephra accumulation. Finally, we also derived combined maps by merging maps of single scenarios with their probability of occurrence as obtained from expert elicitation. Results indicate that in case of a future eruption, even for a moderate-scale one (Violent Strombolian), probability of tephra accumulation larger than 1 kg/m^2 is relatively high (from 21 to 24% considering different model initializations) in the town of Guamote, i.e., the most severely affected site among those tested (43 km W of Sangay). For larger-scale events (i.e., sub-Plinian), the impact of tephra accumulation results to be significant even for the city of Guayaquil (176 km W of Sangay), with probability of tephra accumulation larger than 1 kg/m^2 from 3 to 22% considering different model initializations. For maps combining single maps of historically observed scenarios, the probability (% - [5th-Mean-95th]) of having ≥ 10 kg/m^2 for Guamote is [4-13-25] as maximum values.

Keywords Sangay volcano · Tephra fallout; Probabilistic maps · Uncertainty quantification · PLUME-MoM-TSM · HYSPLIT

Editorial responsibility: S. Massaro

✉ Andrea Bevilacqua
andrea.bevilacqua@ingv.it

1 Istituto Nazionale di Geofisica e Vulcanologia, Sezione di Pisa, via Cesare Battisti 53, 56125 Pisa, Italy

2 Laboratoire Magmas et Volcans, CNRS, IRD, OPGC, Université Clermont Auvergne, 6 Avenue Blaise Pascal, 63178 Aubière, France

3 Instituto Geofísico, Escuela Politécnica Nacional, Ladrón de Guevara E11-253 y Andalucía, Quito, Ecuador

4 Facultad de Ciencias Básicas, Universidad Catolica del Maule, Avenida San Miguel 3605, Talca, Chile

5 Millennium Institute on Volcanic Risk Research – Ckelar Volcanoes, Avenida Angamos 0610, Antofagasta, Chile

6 Laboratoire de Mathématiques Blaise Pascal, CNRS, Université Clermont Auvergne, 3 Place Vasarely, 63178 Aubière, France

Introduction

Tephra accumulation on the ground is undoubtedly one of the major hazard sources from volcanic eruptions, due to its impact over large areas (>100 km^2; Blong 1996) and on many aspects of human life and activities (e.g., farmland/livestock, Annen and Wagner 2003; human health, Baxter and Horwell 2015; electrical infrastructure, Bebbington et al. 2008; roads/transportation systems, Barsotti et al. 2010; buildings stability, Macedonio and Costa 2012; water reservoirs and vegetation, Wilson et al. 2012; crops, Ligot et al. 2024). To cope with such hazards, one of the main tools for both short-term volcanic crises management and long-term urban planning is represented by probabilistic hazard maps. Such products rely on Monte Carlo techniques (Hurst and Smith 2004; Yang et al. 2020) to sample input parameters used to run numerical models of tephra transport and deposition, which are ultimately integrated to create hazard maps (e.g., HAZMAP, Michaud-Dubuy et al. 2021; TEPHRA2, Biass and Bonadonna 2013; FALL3D, Vázquez et al. 2019; VOL-CALPUFF, Barsotti et al. 2018; ASH3D, Barker et al. 2019; HYSPLIT, Tadini et al. 2022). In the context of probabilistic hazard map development, the quantification of the major sources of uncertainty is critically important in the estimation of eruptive source parameters (ESPs) and of the probabilities of occurrence of the identified scenarios, conditional on an eruption occurring within defined temporal frames (Bevilacqua et al. 2016; Sandri et al. 2016; Aravena et al. 2023). Examples for volcanic hazard studies that incorporate strategies of uncertainty quantification and propagation include comparison between available field data and existing global volcanological databases (Biass and Bonadonna 2013), how large is the uncertainty in estimating input parameters from field data (e.g., Biass and Bonadonna 2011; Constantinescu et al. 2022; Yang and Jenkins 2023), how the input uncertainty propagates through the model (e.g., Woodhouse et al. 2015; de' Michieli Vitturi et al. 2016; Tadini et al. 2020), and how it is influenced by wind field variability (e.g., Macedonio et al. 2016; Madankan et al. 2014; Stefanescu et al. 2014). Among the various techniques to quantify uncertainty in the above-mentioned situations, structured expert judgment has revealed to be particularly useful in case few volcanological information is available (see e.g. Neri et al. 2008; 2015; Tadini et al. 2017b; 2021; Bevilacqua et al. 2015; 2022).

In this paper, we present probabilistic tephra fallout hazard maps for Sangay volcano (Ecuador), located ~200 km south of Ecuador's capital city Quito and 175 km to the east of Guayaquil, the main maritime port and commercial capital of the country (Fig. 1). Because of its location, extreme humid weather conditions, and access limited to a difficult two-day trail, Sangay's geology and recent activity are still poorly known (Monzier et al. 1999). For this reason, Sangay volcano has been the topic of a companion study (Bernard et al. 2024) that includes characterization of its eruptive activity and quantification (through an expert elicitation) of the occurrence probability of different eruptive scenarios as well as the probability distribution of their ESPs. The approach described here, similarly to Tadini et al. (2022), utilizes the tephra transport and dispersal model HYSPLIT (Stein et al. 2015) to run a set of simulations whose results

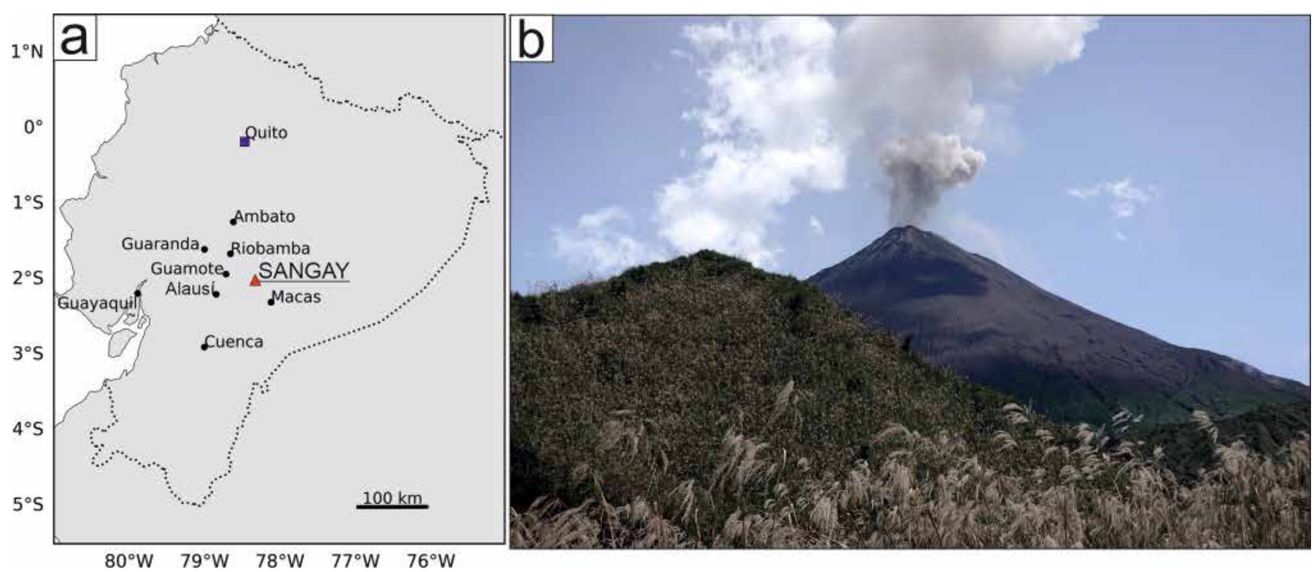

Fig. 1 **a** Location of Sangay volcano (red triangle) in Ecuador (the black dotted line marks national boundaries). The blue square represents the location of the capital city (Quito), and the black dots indicate some towns/cities potentially affected by Sangay volcano tephra fallout. **b** Picture of Sangay volcano on 27/12/2021 (taken from 6 km WSW from the vent)

are then used to produce hazard maps. To improve the representation of the conditions at the volcanic source, we initialized HYSPLIT with the results of the eruption column model PLUME-MoM-TSM (de' Michieli Vitturi and Pardini 2021) through a novel workflow that incorporates uncertainty quantification and propagation by using two different model initializations.

This study is organized as follows. We first summarize the results of Bernard et al. (2024) on Sangay volcano eruptive history and expert elicitation findings in the "Background" section. Then, in the "Methods" section, we describe the modeling strategy, the uncertainty quantification for ESPs and occurrence probability of eruptive scenarios, and the procedure for the production of hazard maps and hazard curves. Finally, the "Results" and "Discussion" sections focus, respectively, on the presentation of the hazard maps/curves and on the discussion of their main implications, while the "Concluding remarks" section draws some final considerations.

Background

Sangay volcano eruptive activity

Bernard et al. (Bernard et al. 2024) classified the activity of Sangay in quiescence, weak eruptive activity, enhanced eruptive activity, and eruptive pulses. This classification is based on the direct observation of the last ~25 years and historical accounts of the last ~400 years.

Quiescence is defined as a state of calm or inactivity for a relatively prolonged period and occurred six times in the 2000–2024 interval (Vasconez et al. 2022). These periods lasted between 5 and 20 months and during them, few isolated ash emissions occurred, whose products impacted only the immediate vicinity (100's m) of the crater and fumarole fields.

Weak eruptive activity is instead the most common behavior of Sangay volcano during the 2000–2024 interval. Bernard et al. (2024) identified two types of weak eruptive activity, namely long-lasting periods (up to several years) and short episodes (few weeks to months). The formers are characterized by a low rate of seismic events (~8–18 per day), a low lava emission rate (~0.3 m^3/s), and SO_2 degassing undetectable by satellite. Short episodes are instead characterized by intermediate seismic event rates (~72–88 per day), intermediate lava emission rates (~0.8–1.5 m^3/s), and low SO_2 degassing (up to 224 t/day). Both are classified as weak eruptive activity because of the absence of impact outside the volcanic cone.

Enhanced eruptive activity has been consistently observed in the 2000–2024 interval and has manifested itself as an increase (from weak activity) in lava emission rate (average 5 m^3/s), in the frequency of explosions (up to 1000 events per day) and, more consistently, in SO_2 degassing (up to 4500 t/day). Enhanced eruptive activity produces frequent ash fallout in local communities, as well as increased sedimentation in rivers flowing down from the volcano.

Finally, *eruptive pulses*, which occur at a much shorter time scale than the previous types of activity, are predominantly explosive and have been classified by Bernard et al. (2024) in four categories (from small to large size): Strong Ash Venting (*SAV*), Violent Strombolian (*VS*), sub-Plinian (*SPL*), and Plinian (*PL*). Among them, only the first two categories have been observed over the past 20 years. *SAV* events have frequently been associated with peaks of lava emission rate and PDCs formation (Vasconez et al. 2022; Bernard et al. 2024; Hidalgo et al. 2022) and lasted for hours to days with bent column height < 5 km above crater and sometimes higher (up to 8 km above crater) pulsatile gas plumes. During *SAV* events, ash clouds frequently reached more than 100 km from Sangay (Moran-Zuloaga et al. 2023). *VS* in the past 20 years only occurred between September 2020 and May 2021 and are easily spotted on both local and regional seismic records (Bernard et al. 2022; Moran-Zuloaga et al. 2023; Bernard et al. 2024). They have been associated with large SO_2 emissions (up to > 45,000 t/day), high lava emission rate (>20 m^3/s), and PDCs formation. According to the monitoring data, *VS* events lasted between 2 and 6 h with eruptive plumes that generated column height of 5–10 km above the crater which created wide umbrella-shaped ash clouds. One *SPL* has occurred during the past 400 years (in 1628 CE) and one Holocene *PL* pulse has been recognized based on a 2–20-cm-thick dacitic tephra fallout deposit, 1 m beneath the current soil, found up to ~20 km from the volcano (see Bernard et al. 2024).

Given the few constraints on the occurrence of *PL* eruptions at Sangay, in the following sections, we first present the maps and the analyses for the *SAV*, *VS*, and *SPL* scenarios only, which are the eruption scenarios historically observed over the past ~20 (SAV and VS) and ~400 (SPL) years. In the discussion, we also present the results when considering the *PL* scenario.

Expert elicitation for eruptive scenarios at Sangay volcano

To quantify the uncertainty associated with the eruptive scenarios of Sangay volcano (described in the previous section), a performance-based expert elicitation session was conducted in 2021 (see Aspinall 2006; Aspinall and Cooke 2013 for generalities on expert elicitation and Bernard et al. 2024 for more details on the Sangay elicitation). Eighteen experts took part in this exercise and were asked to give their judgments on:

- the probability, for each scenario, of Sangay experiencing at least one eruption in two different timeframes, namely 10 years and 100 years in the future;
- the probability distribution, for each scenario, of three eruptive source parameters, namely, the average height of the column during the pulse (in km above the crater), the total volume of the fallout deposit emitted during the pulse (in 10^6 m^3) considering an equivalent deposit density of 1000 kg/m^3, and the average duration of the eruption as detected by geophysical monitoring (in hours).

For all these questions and after carefully considering all the evidence and data presented during the meeting, experts provided their judgments as the 5^{th}/Median/95^{th} percentile values of a probability distribution. Individual experts' answers for target questions were then pooled together by using an equal weights rule and two independent performance-based models (Classical Model, Cooke 1991; ERF, Flandoli et al. 2011). In the following, we adopt the results based on the Classical Model; for more information on the other approaches, see Bernard et al. (2024). To derive the pooled probability density functions for each question (representing the view of the group in the form of a new virtual expert, called "Decision Maker"), individual experts' answers were sampled 10,000 times (de' Michieli Vitturi et al. 2024).

Results of the probability for the four scenarios for the next 100 years (utilized for map combination, see the "Type of outputs" section) are displayed in Fig. 2. Note that we plot probability density functions of occurrence probabilities, i.e., uncertainty distributions of probability estimates, according to a doubly stochastic approach (Tadini et al. 2017a; Bevilacqua et al. 2018; 2021). Results of the three eruptive source parameters for the four scenarios (utilized in the "Simulation setting" section) are instead displayed in Fig. 3.

Methods

Numerical models and workflow for map production

The HYSPLIT (Hybrid Single-Particle Lagrangian Integrated Trajectory) model was used to simulate the

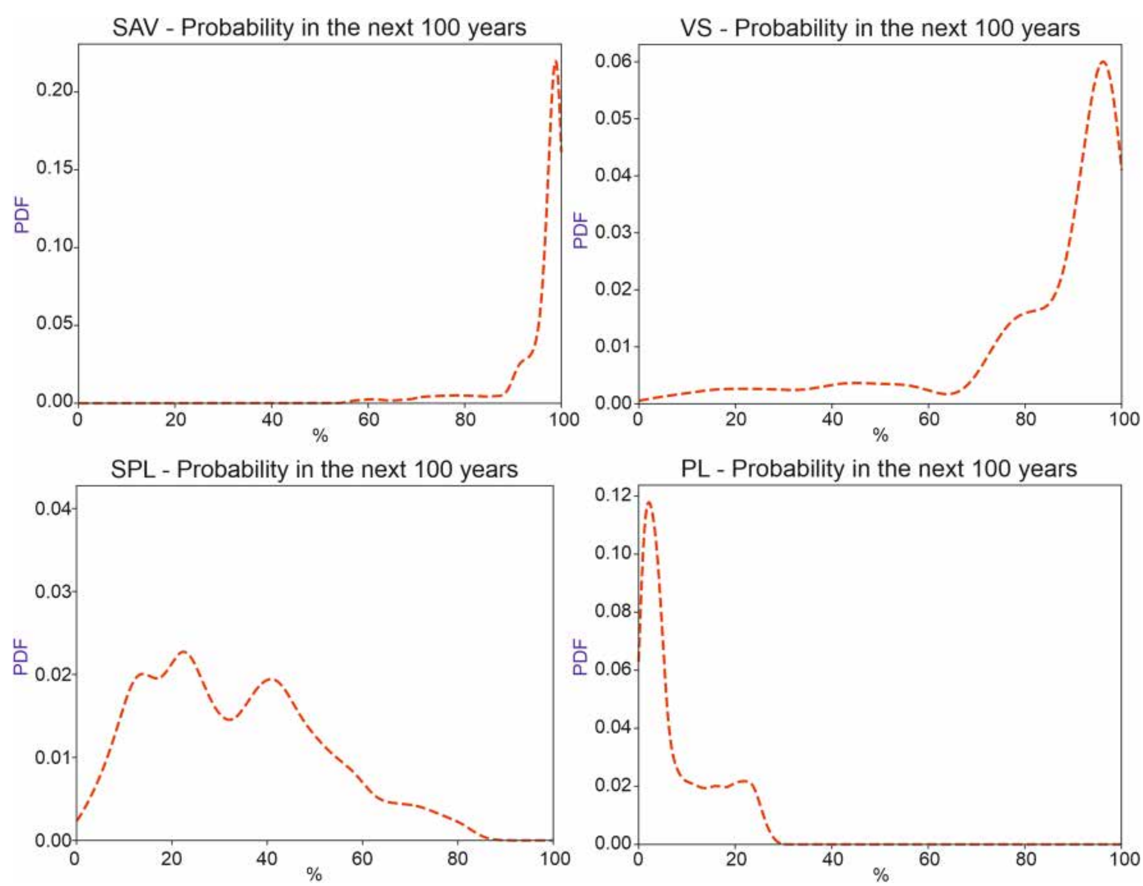

Fig. 2 Probability density functions (PDF) of the uncertainty on the probability (for each scenario, SAV, VS, SPL, PL) of having at least one eruption in the next 100 years (Bernard et al. 2024)

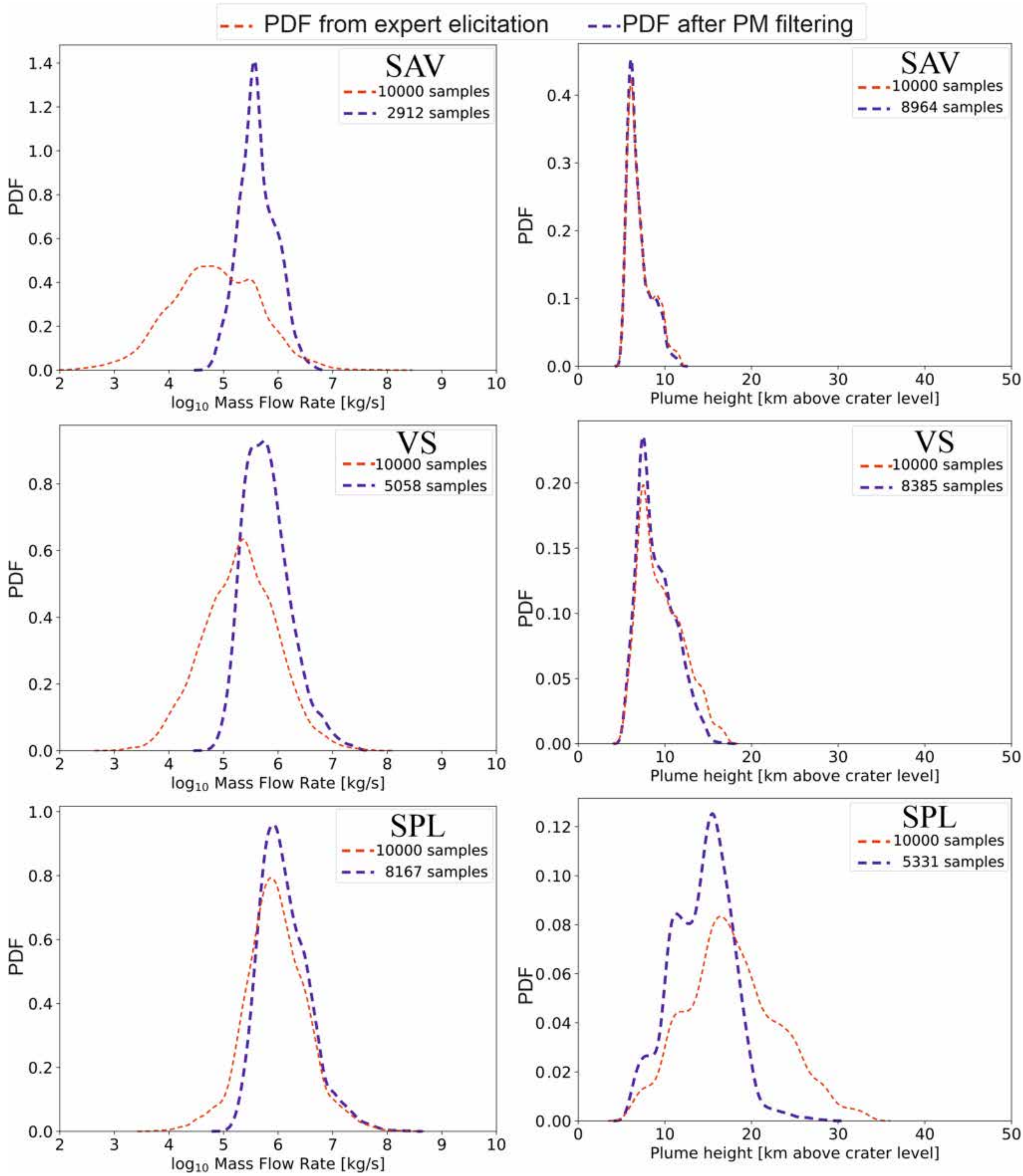

Fig. 3 Probability density functions of mass flow rate (expressed as $\log_{10}$) and plume height (in km above crater) of the SAV, VS, and SPL eruptive scenarios. The figure refers to model initialization with total volume (tv) and the filtering done considering the plume height (ph) (left panels) and model initialization with ph and the filtering done considering the tv (obtained from mass flow rate from the model, converted into total mass considering eruption duration, and finally converted into total volume; right panels). In each panel, the red dashed line indicates the original density distribution obtained from the 10,000 samples produced from the results of the elicitation, while the blue dashed line indicates the filtered density distribution obtained from the samples that passed the control (by running PLUME-MoM-TSM only). The 1200 simulations were taken from this latter distribution. Details on the filtering approach are provided in the "Simulation setting" section

atmospheric dispersion of tephra particles and their deposition on the ground (Stein et al. 2015). HYSPLIT has been extensively utilized for both research and operational purposes, with some Volcanic Ash Advisory Centers relying on it as a standard model (Mastin et al. 2017). In order to execute the numerical simulations, the model requires inputs on meteorological conditions and on the tephra injection rates in the atmosphere. Meteorological conditions are supplied as a dataset where the parameters describing the evolution of the atmospheric properties in space and time are listed on a 3D grid. Wind speed and direction are the main parameters controlling the transport and deposition on the ground of tephra particles. Tephra injection conditions, describing how tephra particles are released into the atmosphere (including factors such as amount, duration, and vertical distribution), also need to be defined as inputs. To this aim, we coupled HYSPLIT with the 1D steady-state eruption column model PLUME-MoM-TSM (two-size moment - de' Michieli Vitturi and Pardini 2021). PLUME-MoM-TSM simulates the ascent of an eruption mixture through the atmosphere from the vent source until it reaches its maximum height, accounting for wind effects and simulating the umbrella cloud spreading at the neutral buoyancy height. Tephra particles lost from the column below the neutral buoyancy height are injected into the atmosphere from pointwise sources located on the plume axis. Particles reaching the neutral buoyancy enter the atmosphere through a circular area source which best fits the position and upwind spreading of the umbrella cloud. Once in the atmosphere, particle transport and deposition on the ground is simulated by HYSPLIT based on the assumed particle properties and the characteristics of the wind field. The coupling between PLUME-MoM-TSM and HYSPLIT is done through Python scripts that allow the results of PLUME-MoM-TSM to be automatically used to generate the input file for HYSPLIT. A detailed description of this procedure, together with several applications, can be found in Pardini et al. (2020) and Tadini et al. (2020). We note that PLUME-MoM-TSM can be initialized with either mass flow rate or the maximum column height, in both cases by taking into account atmospheric conditions. In the latter case, an inversion step is performed to retrieve the conditions at the vent (initial velocity and plume radius) that correspond to a mass flow rate capable of generating a column with the desired height.

In this study, we applied the above-mentioned models to produce probabilistic maps of tephra accumulation on the ground for Sangay volcano. To achieve this, we developed a numerical workflow that automatically runs an ensemble of thousands of simulations, i.e., a Monte Carlo simulation, where each ensemble member is initialized with a specific set of ESPs and meteorological conditions. Eruption conditions include mass eruption rate (or column height), eruption duration, and physical properties of the tephra particles, such as size, shape, and density. ESPs of each ensemble member can be either fixed values common to all the members or random values sampled from pre-defined probability density functions. Indeed, some eruption parameters are more difficult to constrain than others and/or have a higher impact on model results. These considerations guided the selection of the parameters that could be treated as fixed and equal among all the ensemble members, as well as those best defined by using probability density distributions to assign different values to each ensemble member. Probability density distributions were derived from a literature review and/or from a Monte Carlo sampling of the results of the expert elicitation described above. Finally, to account for the uncertainty on meteorological conditions, the eruption onset time of each ensemble member was randomly sampled in the period 2012–2022, taking into account seasonal variability by having the same number of samples within each month of the considered period. The assumption behind this choice is that the last decade of meteorological conditions is appropriate to statistically capture the main features of atmospheric circulation in the coming decades. In addition, our sampling time window fully overlaps with those of recent similar studies, which consider time windows ranging from 6 to 29 years (Bonasia et al. 2011, 2014; Titos et al. 2022).

Once the appropriate set of initial conditions are defined for each ensemble member, the numerical simulations are executed and processed to produce the outcomes of interest which, in our case, are probabilistic hazard maps and curves (see the "Type of outputs" section).

Simulation setting

The domain considered in the tephra hazard assessment has a vertical extension of 50 km above ground and covers the entire Ecuador, spanning from 5.5°S to 1.5°N in latitude and from 81.0°W to 75.0°W in longitude, as shown in Fig. 1. The numerical simulations in HYSPLIT were performed on a grid with horizontal resolution of 0.05° (approximately 5 km). The adopted meteorological information derives from the ERA5 dataset (Hersbach et al. 2020) supplied by the European Centre for Medium-Range Weather Forecasts (ECMWF). ERA5 is a reanalysis dataset for the global weather with data available from 1940. Data is gridded hourly with a horizontal resolution of 0.25° × 0.25° (approximately 27–28 km in latitude and longitude at the equator) and 37 vertical pressure levels (from 1000 to 1 hPa). A dataset covering 10 years from 2012 to 2022 was used to perform the numerical simulations, under the assumption that such dataset is appropriate for evaluating the hazard due to future eruptions at Sangay volcano. As a preliminary analysis, wind rose diagrams (for ERA5 data) showing wind speed and direction at the Sangay volcano location were constructed for different height intervals from

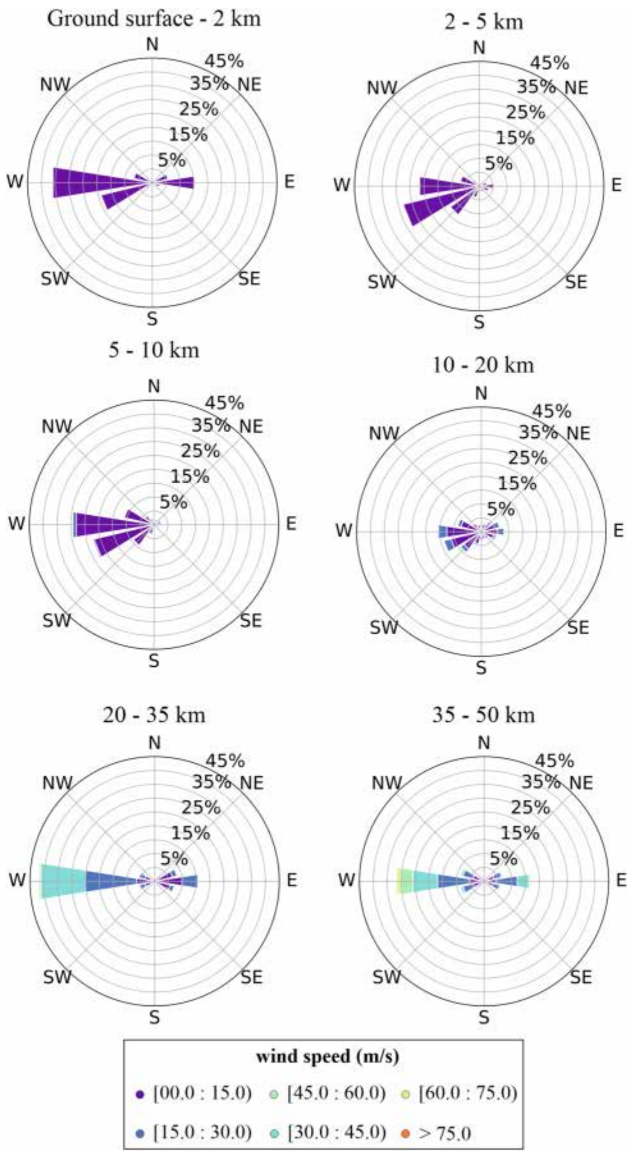

Fig. 4 Wind rose diagrams at the Sangay volcano location (2.00°S; 78.32°W), constructed from the ERA5 reanalysis dataset covering the years from 2012 to 2022. Wind speed and direction were evaluated for different height intervals above the crater: surface–2 km, 2–5 km, 5–10 km, 10–20 km, 20–35 km, and 35–50 km. Note that the diagrams show the direction toward which the wind blows

the topographic surface to 50 km (Fig. 4). It emerges that the wind mainly blows toward the west for all the considered height intervals. The greatest spread in wind direction is observed from 10 to 20 km, where wind appears to blow in sectors NW-W and W-SW, with a lesser extent toward the east. A strong dominance of the winds blowing toward the west is clearly observed at the highest heights (20–35 km and 35–50 km), with a smaller extent observed in the eastward direction. For these latter two heights, a seasonal analysis for, respectively, dry season (Oct–May) and wet season (Jun–Sep) does not evidence a preferential seasonal dominance for the 20–35-km range, while for the 35–50-km range, stronger winds tend to blow more frequently toward W in the wet season, although in the dry season there is still a prevalence of W-blowing winds (see Fig. 1S from Supporting Information 2). Since typical neutral buoyancy levels for our four eruption types are located between 10 and 35–40 km (see e.g. Mastin et al. 2009), we provide wind pattern of the 1200 simulations for the SAV and PL eruption types in Figs. 2S-3S for the 10–20-, 20–35-, and 35–50-km ranges. From the analysis of these diagrams (results are the same also for the VS and SPL eruptions), we could conclude that our samples fully capture the variability of the wind pattern of the whole dataset.

The definition of the eruption conditions of the four investigated scenarios (SAV, VS, SPL, and PL) was based on both literature review and expert elicitation. The parameters defined through probability density distributions are as follows: eruption duration, total mass of the deposit, plume height, and total grain size distribution (TGSD). The remaining parameters were fixed for all the ensemble members, and a complete list can be found in Supporting Information 1. The uncertainty on the TGSD was based on literature review. In particular, TGSD was assumed independent from eruption size (given the few constraints available for TGSD at Sangay, especially from proximal deposits—see Bernard et al. 2022) and as a lognormal distribution defined by a mean value μ and a standard deviation σ. Both μ and σ were considered uncertain and defined as uniform distributions in the ranges $[-1; 3]$ φ for μ and $[2; 3]$ φ for σ. Eruption duration, total mass of the deposit, and plume height were supplied by the elicited distributions in Bernard et al. (2024).

An initial set of 10000 samples for each eruption scenario was produced by independently sampling the distributions of eruption duration, total volume of the deposit (converted into mass considering 1000 kg/m^2 as deposit density), plume height, μ, and σ. Since mass flow rate was not directly supplied by the elicitation, for each of the 10,000 samples, we computed the corresponding average mass flow rate by converting the total deposit volume into total mass (with an additional 5% mass to account for magma water content) and dividing this latter by the duration of the eruption.

As stated above, the eruption column model can be initialized with either total volume or column height. Therefore, for each scenario, we performed two sets of numerical simulations using either one of the initialization schemes. In order to have a good compromise between statistically meaningful outputs and acceptable computational times, for each eruption scenario and initialization scheme, we performed 1200 simulations by running PLUME-MoM-TSM and HYSPLIT. The eruption parameters used to initialize the 1200 simulations are a subset of the original 10,000 samples, and a preliminary analysis was done to ensure consistency between the

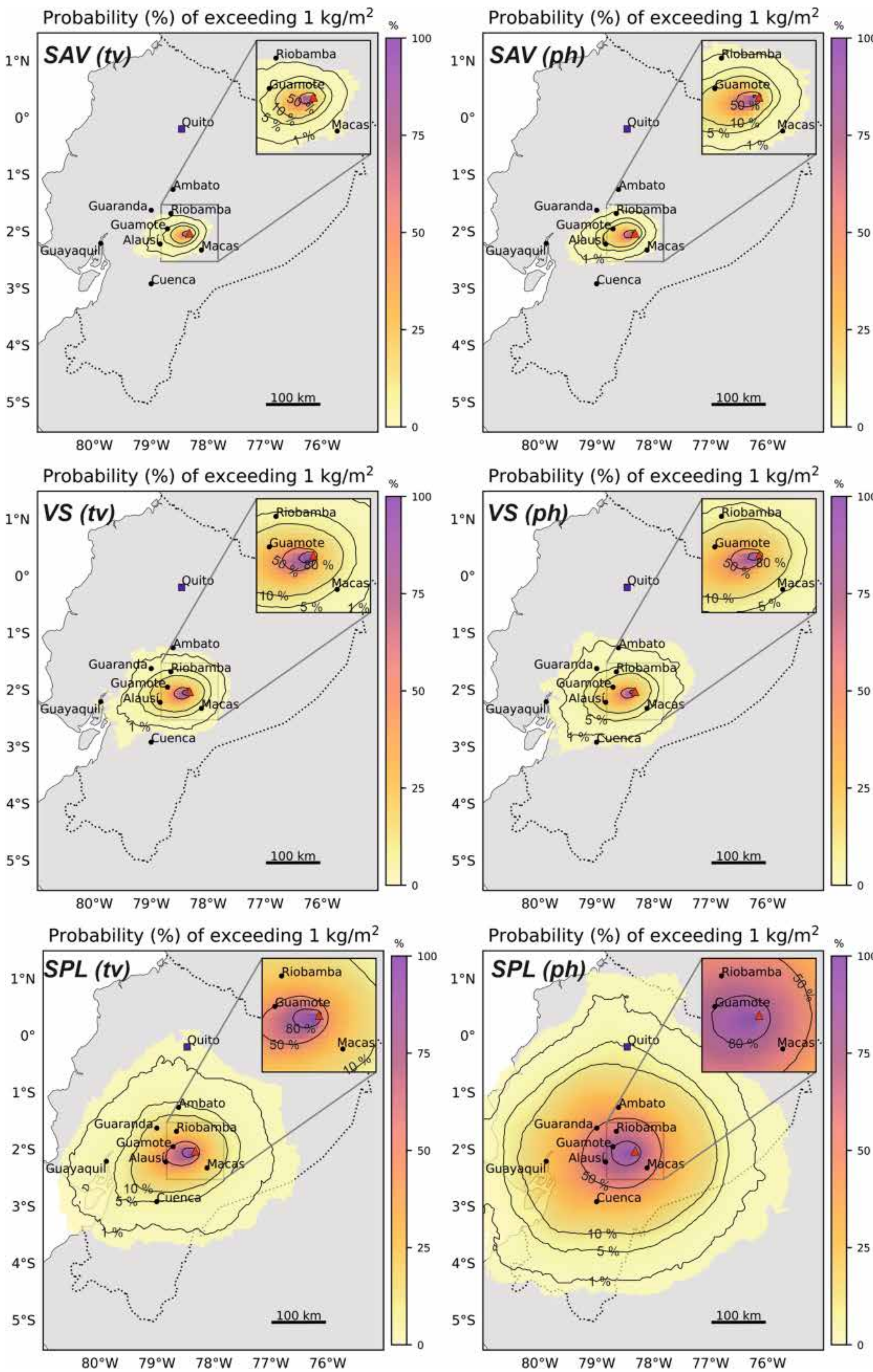
Probability (%) of exceeding 1 kg/m²
SAV (tv)
SAV (ph)
VS (tv)
VS (ph)
SPL (tv)
SPL (ph)
Quito
Ambato
Guaranda
Riobamba
Guamote
Alausí
Macas
Guayaquil
Cuenca
100 km
1°N
0°
1°S
2°S
3°S
4°S
5°S
80°W
79°W
78°W
77°W
76°W
%
100
75
50
25
0
1 %
5 %
10 %
50 %
80 %

◂**Fig. 5** Sangay tephra fallout hazard maps for SAV, VS, and SPL scenarios for 1 kg/m^2 threshold. Maps in the left column are produced initializing PLUME-MoM-TSM with total volume (tv), whereas those in the right column by using plume height (ph). Contour lines, where not indicated, follow the progression 1%, 5%, 10%, 50%, and 80%

parameters values used to initialize the models and the results of the elicitation. This analysis consisted in running PLUME-MoM-TSM only (without HYSPLIT) over the entire set of 10000 samples and rejecting the samples whose numerical results were inconsistent with the results of the elicitation.

In particular, for the simulations initialized with the total volume (tv), we rejected the simulations giving as output a value of plume height outside the range of values of the corresponding elicited distribution. Similarly, for the simulations initialized with plume height (ph), we rejected those producing a total volume erupted outside the range of the elicited distribution. We remark that we did this analysis for each eruption scenario and initialization scheme.

Figure 3 illustrates the comparison between the original distributions formed by the 10,000 samples (red dashed lines) and the filtered distributions of the "accepted" samples (blue dashed lines). The 1200 simulations are randomly sampled from these latter distributions. For the simulations initialized with tv (left panels in Fig. 3), 2912 and 5058 samples passed the check, respectively, in the SAV and VS scenarios. In particular, in the SAV scenario, the majority of samples has a mass flow rate (and a total deposit volume) lower than those consistent with the elicited plume height. In the SPL and PL scenarios, a higher proportion of samples passed the check, with 8167 samples in the SPL scenario and 9129 in the PL scenario (for PL, see Fig. 19S from Supporting Information 2). These results indicate a good agreement between the elicited deposit volumes and plume heights in these scenarios. Regarding the simulations initialized with ph (right panels in Fig. 3), it emerged that ca. 80–90% of samples passed the check for the SAV (8964) and VS (8385) scenarios, while 5331 samples were accepted in the SPL scenario. In the PL scenario (see Fig. 19S from Supporting Information 2), 8686 samples passed the filtering step. This filtering approach mitigated the independence of the 10,000 samples of eruptive source parameters, especially between mass flow rate (derived from total volume) and column height and, at a lower degree, with respect to the previous two parameters and eruption duration. The only purely independent parameter is TGSD, whose effect in the final results has been assumed secondary with respect to the other inputs. Future studies with more quantitative data on TGSD for Sangay volcano could help in updating our results.

To associate meteorological conditions with each ensemble member, the start date and time of the eruptions were randomly sampled from 2012 to 2022 (the start and end years of the ERA5 dataset). The end dates of the eruptions were derived from their durations, and the numerical runs continued for additional 24 h after the end of each eruption to achieve complete tephra deposition on the ground. To guarantee a uniform representation across all months, the meteorological dataset was sampled to initialize 100 simulations each month, totaling 1200 simulations.

Type of outputs

The outcomes that we produced by running a Monte Carlo simulation consisting of an ensemble of 1200 members are probabilistic hazard maps and curves for tephra accumulation on the ground.

Hazard maps cover the entire domain considered in the simulations and show the probability of exceeding specific thresholds of ground load. They are obtained by calculating the probability $P\tau$ that the ground load at each pixel $N_{x,y}$ of the computational grid exceeds a certain ground load threshold (τ). $P\tau$ is determined by counting the number of times (n_i) τ is exceeded by the ground load resulting from each simulation of the ensemble (GL_i), and then dividing by the total number m of simulations:

$$P_\tau(N_{x,y}) = \frac{\sum_{i=1}^{m} n_i}{m} \tag{1}$$

where

$$n_i = \begin{cases} 1, & if\left[GLi\,(N_{x,y}) \geq \tau\right] \\ 0, & otherwise \end{cases} \tag{2}$$

In this study, in order to obtain a set of results able to provide useful information about the potential impacts (Jenkins et al. 2015), we adopted four threshold values: 0.1, 1, 10, and 100 kg/m^2. These thresholds were chosen as they can be associated to various degrees of damage and disruption to communities and particularly:

- 0.1 kg/m^2 is sufficient enough to be detectable by residents and might cause minor vegetation damage and the covering of road markings (Magill et al. 2013).
- 1 kg/m^2 may lead to airport closure, contamination of water supplies, damage of electrical appliances, disruption of road, rail, and air transport, and respiratory problems (Jenkins et al. 2012).
- 10 kg/m^2 cause minor structural damage for weaker building and major damage on crop and vegetation (Jenkins et al. 2012).
- 100 kg/m^2 may cause partial or total collapse of several buildings (Jenkins et al. 2012).

Hazard curves, instead, are local results computed at specific locations of interest. For each investigated location, the corresponding hazard curve indicates the exceedance probability EP = Pr(GL > *X*), where GL is the ground load computed from the simulations and *X* is a specific value within a certain interval. To derive such curves, outputs of ground load GLi resulting from the *m* simulations are sorted in ascending order (GL_0, GL_1, GL_2,...GL_{m-1}), while the exceedance probability EPi is computed as follows (following Bonadonna 2006):

$$EP_i = 1 - \frac{i}{m}, for 0 \le i < m \quad (3)$$

The locations chosen to compute the hazard curves are those reported in Fig. 1 and include the capital city of Ecuador, Quito, as well as some main cities/towns located within 200 km from Sangay volcano.

All maps and curves are produced for either single scenarios and combined scenarios. In this latter case, we consider the uncertainty distribution of the probability of having at least one eruption among each scenario in the next 100 years (Fig. 2); the resulting maps/curves are related to the occurrence, for each scenario, of the largest event within the next 100 years, excluding replication of the same event and cumulative tephra load by multiple events. The combination of maps and curves was done, respectively, for the SAV and VS, for the SAV, VS, and SPL, and for the SAV, VS, SPL, and PL joint scenarios. For example, to obtain the hazard maps of the SAV-VS-SPL-PL (the others are similar in the approach), we start from the probabilistic maps (H) of the four scenarios and the 10,000 samples defining the distributions of probabilities (P) of SAV, VS, SPL, and PL for the next 100 years (Fig. 2). For each sample, we combine the four scenarios as follows:

$$\begin{aligned} H_{comb} = {} & P_{SAV} * (1 - P_{VS}) * (1 - P_{SPL}) * (1 - P_{PL}) * H_{SAV} \\ & + P_{VS} * (1 - P_{SPL}) * (1 - P_{PL}) * H_{VS} \\ & + P_{SPL} * (1 - P_{PL}) * H_{SPL} + P_{PL} * H_{PL} \end{aligned} \quad (4)$$

By applying Eq. (4) for each of the 10,000 samples defining the distributions of probabilities, we obtain 10,000 maps/curves and from these latter, we show those representing the mean value and the $5^{th}/95^{th}$ percentiles to illustrate the uncertainty associated with the map combination. We then applied the same approach to derive the combined hazard curves (representing the mean value and the $5^{th}/95^{th}$ percentiles) for each location.

Results

In this section, we present, in the single eruptive scenarios, the hazard maps for the 1 kg/m^2 threshold and the hazard curves for all sites. Then, we present, in the combined SAV-VS-SPL and SAV-VS-SPL-PL scenarios, hazard maps for the 1 kg/m^2 threshold and hazard curves for Guamote, Guayaquil, and Macas. The remaining maps (0.1, 10, and 100 kg/m^2) and curves (combined scenarios for the remaining six sites) are available in Supporting Information 2. Moreover, interpolated values at 0.1, 1, 10, and 100 kg/m^2 for all the hazard curves are available in Supporting Information 3. We also provide ASCII Arc/Info files for all maps in Supporting Information 4.

Hazard maps/curves in the single scenarios (SAV, VS, and SPL)

By looking at the maps (Fig. 5), the curves (Fig. 6), and the interpolated values of the hazard curves (Supporting Information 3) for single scenarios, we note that, between the two initialization setups, differences tend to be higher with increasing the size of the eruption (i.e., larger in the SPL than in the SAV/VS). For example, considering the 1 kg/m^2 and the interpolated probabilities of hazard curves, we observe that differences between initialization setups at all sites are of maximum ~12% in the SAV/VS, while they could reach up to ~40% for the SPL. Regarding the sites for which we produced hazard curves (Fig. 6), Guamote (located ~43 km W of Sangay) is the town that, on average, would suffer more tephra accumulation (probability of tephra accumulation of 1 kg/m^2 between 4.6 and 78% in the three scenarios, see Supporting Information 3). We stress that at Guamote, even in case of a moderate-size eruption such as a VS, the probability of having a ground load of 1 kg/m^2 is relatively high (i.e., 21–24%). For the same eruption type, the town of Alausí (~60 km SW of Sangay) would also be affected with similar probabilities (16–18%), while the two largest cities in Ecuador (Quito and Guayaquil) would suffer a potential tephra accumulation of 1 kg/m^2 mostly for a SPL eruption type with, respectively, 0.7–6% and 3–22% probability.

Hazard maps/curves for combined scenarios (SAV, VS, and SPL)

Figures 7 and 8 show, respectively, the hazard maps of the 1 kg/m^2 threshold and the hazard curves (for Guamote, Guayaquil and Macas towns) related to the combined SAV, VS, and SPL, which are the eruptive styles actually observed over the last 20 years (SAV and VS) and 400 years (SPL), respectively (for the 0.1, 10, and 100 kg/m^2 thresholds, please refer to Figs. 7S-9S from Supporting Information 2; hazard curves for the remaining 6 sites are reported in Figs. 10S-11S from Supporting Information 2). For completeness, we also report in Supporting

Information 2 (Figs. 12S-18S) hazard maps and curves of combined smallest-scale styles (SAV and VS). Even in this case (similarly to the "*Hazard maps/curves in the single scenarios (SAV, VS, and SPL)*" section), we note that differences between the different adopted initialization setups could be relevant (reaching up to 40% from the sites where hazard curves were produced, see Supporting Information 3).

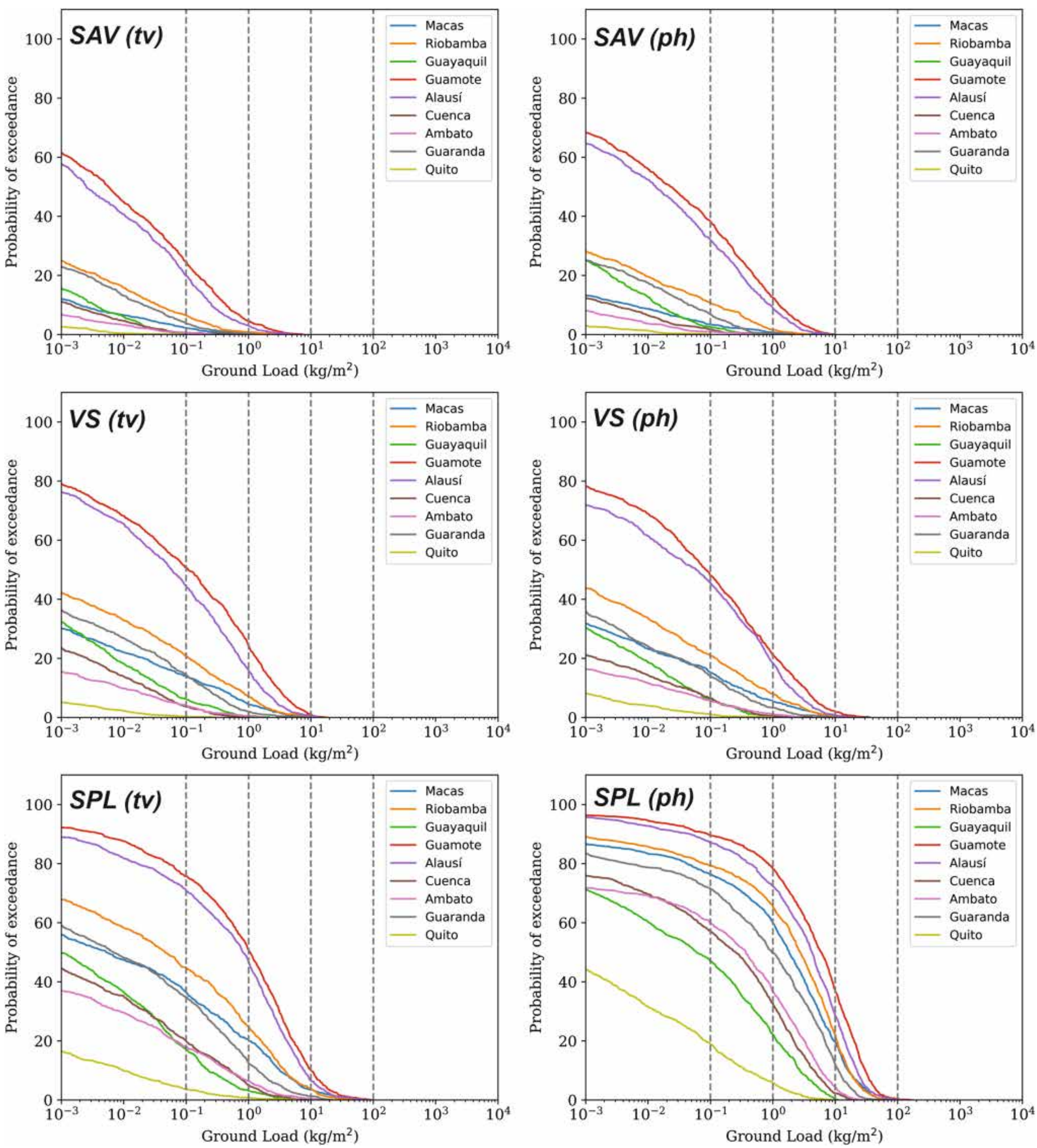

Fig. 6 Hazard curves for 9 sites (see Fig. 1) for the SAV, VS, and SPL scenarios. Curves in the left columns are produced by initializing PLUME-MoM-TSM with total volume (tv), whereas those in the right column by using plume height (ph). Interpolated values at 0.1, 1, 10, and 100 kg/m^2 are reported in Supporting Information 3

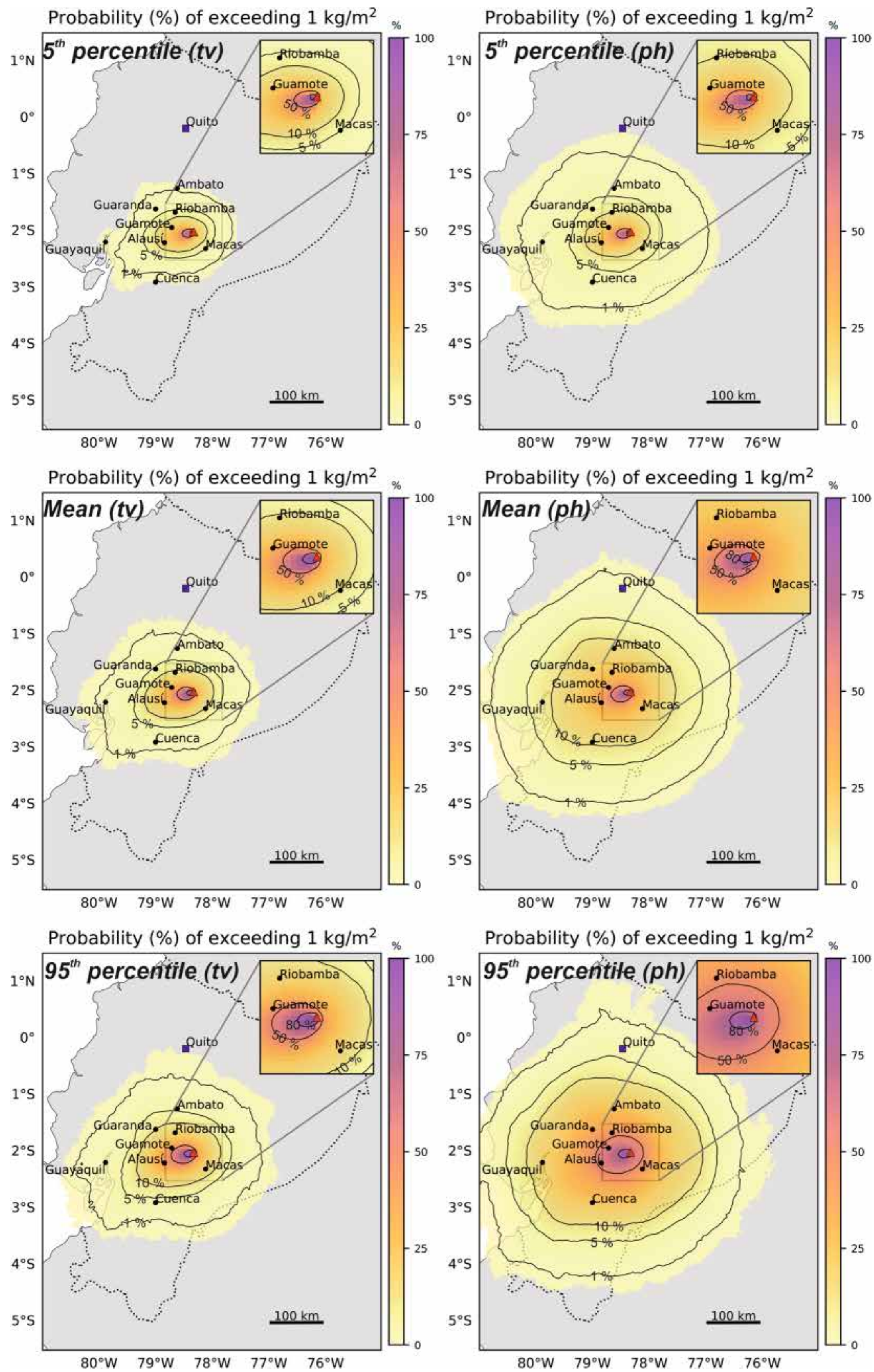
Probability (%) of exceeding 1 kg/m²
5th percentile (tv)
5th percentile (ph)
Mean (tv)
Mean (ph)
95th percentile (tv)
95th percentile (ph)
Riobamba
Guamote
Macas
Quito
Ambato
Guaranda
Alausí
Guayaquil
Cuenca
100 km
1 %
5 %
10 %
50 %
80 %
1°N
0°
1°S
2°S
3°S
4°S
5°S
80°W
79°W
78°W
77°W
76°W
%
0
25
50
75
100

◂**Fig. 7** Sangay tephra fallout hazard maps for the combined SAV, VS, and SPL scenarios for 1 kg/m^2 threshold corresponding to the 5th percentile, the mean, and the 95th percentile. Maps in the left column are produced initializing PLUME-MoM-TSM with total volume (tv), whereas those in the right column using plume height (ph). Contour lines, where not indicated, follow the progression 1%, 5%, 10%, 50%, and 80%

Combined maps when considering the Plinian (PL) event

In the previous section, we have presented maps of the combined SAV, VS, and SPL scenarios, as they represent eruptions that occurred at historical and recent times. However, the PL scenario has also been considered by Bernard et al. (2024) due to the presence of a tephra deposit associated with the Holocene eruptive history of Sangay that is consistent with a Plinian event. The expert elicitation outcome assigned to this scenario a median probability of occurrence within the next 100 years of ~1%, but with an upper uncertainty bound (95th percentile) of ~20%. In Fig. 9, we report both the hazard maps (1 kg/m^2 threshold, for the other thresholds see Fig. 18S from Supporting Information 2) and the hazard curves of this scenario for the two initialization setups, where we can easily observe that differences between the two setups are sometimes high (i.e., up to ~40% when comparing interpolated probabilities from hazard curves, see Supporting Information 3).

Figures 10 and 11 display the maps (1 kg/m^2) and curves (Guamote Guayaquil, Macas) of the four combined scenarios (for other thresholds and sites, please refer to Figs. 21S-25S from Supporting Information 2). The maps/curves with only three scenarios (Figs. 7 and 8) exhibit larger differences for more distal location with respect to vent area and proximal locations (see for instance the hazard curve for the town of Guamote). Differences are also more pronounced between the maps/curves with the initialization tv (when compared with those produced with an initialization based on ph) and between maps/curves referred to the 95th percentile (as compared to the mean and the 5th percentile). For example, for the town of Guamote and the 1 kg/m^2 threshold (see Supporting Information 3), the difference between the 95th percentile probabilities of the tv curves is ~18%, while differences between the means and the 5th percentiles are, respectively, ~8% and ~3%. Conversely, for the ph curves, differences for the 5th percentiles, means, and 95th percentiles are, respectively, ~3%, ~4%, and ~6%. Such differences are proportionally similar for the other sites.

Average differences are around ~6% for all sites, thresholds, percentiles, and initialization setups, while a maximum difference of ~28% is computed for the Ambato site, tv initialization, threshold 0.1 kg/m^2 and 95th percentile. For comparison, average differences between the SAV-VS-SPL and the SAV-VS interpolated values is ~9% for all sites, thresholds, percentiles, and initialization setups, while the maximum difference is ~40% for Macas site, ph initialization, threshold 0.1 kg/m^2, and 95th percentile.

Discussion

Comparison of hazard maps with historical observations and existing hazard maps

The results presented in the previous sections can be compared both to observed mass loadings at key locations during recent eruptions and to existing hazard maps. With respect to the former, Bernard et al. (2022) provided a detailed description of the VS eruptive event of September 20, 2022. During this pulse, ground load was measured in some sites for which we have produced hazard maps, e.g., Guamote, Alausí, and Guayaquil. Values for these three locations are, respectively, 0.19, 0.175, and 0.02 kg/m^2: in the same locations, hazard curves of the VS eruptive pulse (Fig. 7) showed probability of exceeding the same values of ~50%, ~45%, and ~20%. Our results are therefore in accordance with these observations.

To further compare our results with actual observations, we provide some new data about ground load measured at 5 towns (Alausí, Guamote, Guaranda, Guayaquil, and Riobamba, see Fig. 1) during 12 eruptive pulses (8 SAV and 4 VS) occurred between June 2020 and June 2024 (Table 1). These data, although based on a relatively small number of events, allow to count the number of eruptions which caused, in each location, a ground load larger than 0.1 and 1 kg/m^2, and to compare them with a binomial model using the probability of exceeding the same thresholds conditioned on the occurrence of either SAV or VS eruptions for the two initializations (mfr and ph) as interpolated from the hazard curves (see Supporting Information 3). This comparison is presented in Table 2, and the binomial likelihoods of the best performing initializations in each location are all above 25%, with peaks above 95% in several cases. These statistics are not enough for validating our approach, but we could appreciate that our modeling results associate significant likelihood to the real observations.

We remind, however, that for the smallest tephra accumulation values (0.1 and 1 kg/m^2), corresponding to about 0.1, 1 mm of deposit, the ash is very easily remobilized by the local winds, producing large spatial variations. In this context, these tephra loading can be considered only as average values valid on a relatively large area, with local variations that may reach one or more orders of magnitude.

The current official IG-EPN hazard maps for Sangay volcano has been developed by Ordoñez et al. (2011). In this map, two areas potentially affected by tephra fallout were identified with respect to two scenarios (“small” and

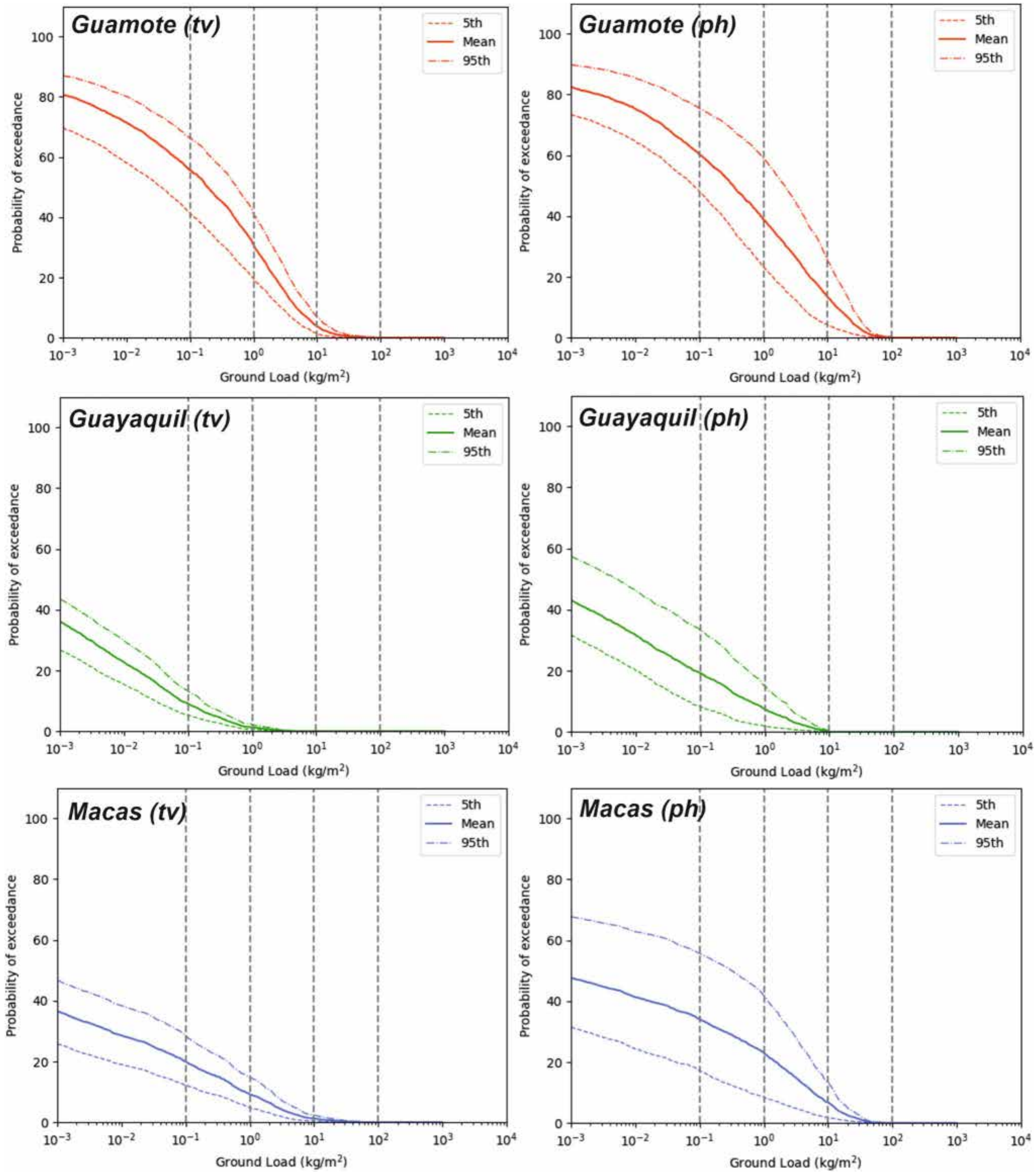

Fig. 8 Hazard curves for three sites (Guamote, Guayaquil, and Macas, see Fig. 1) for the combined SAV, VS, and SPL scenarios corresponding to the 5th percentile, the mean, and the 95th percentile. Curves in the left column are produced by initializing PLUME-MoM-TSM with total volume (tv), whereas those in the right column by using plume height (ph). Interpolated values at 0.1, 1, 10, and 100 kg/m^2 are reported in Supporting Information 3

"moderate," roughly corresponding to SAV and VS, respectively) and modeled with fixed ESPSs and random wind directions/velocities. Although a detailed comparison with respect to our fully probabilistic results is not straightforward, we note that in the official IG-EPN map, the area potentially affected by tephra fallout for moderate eruption

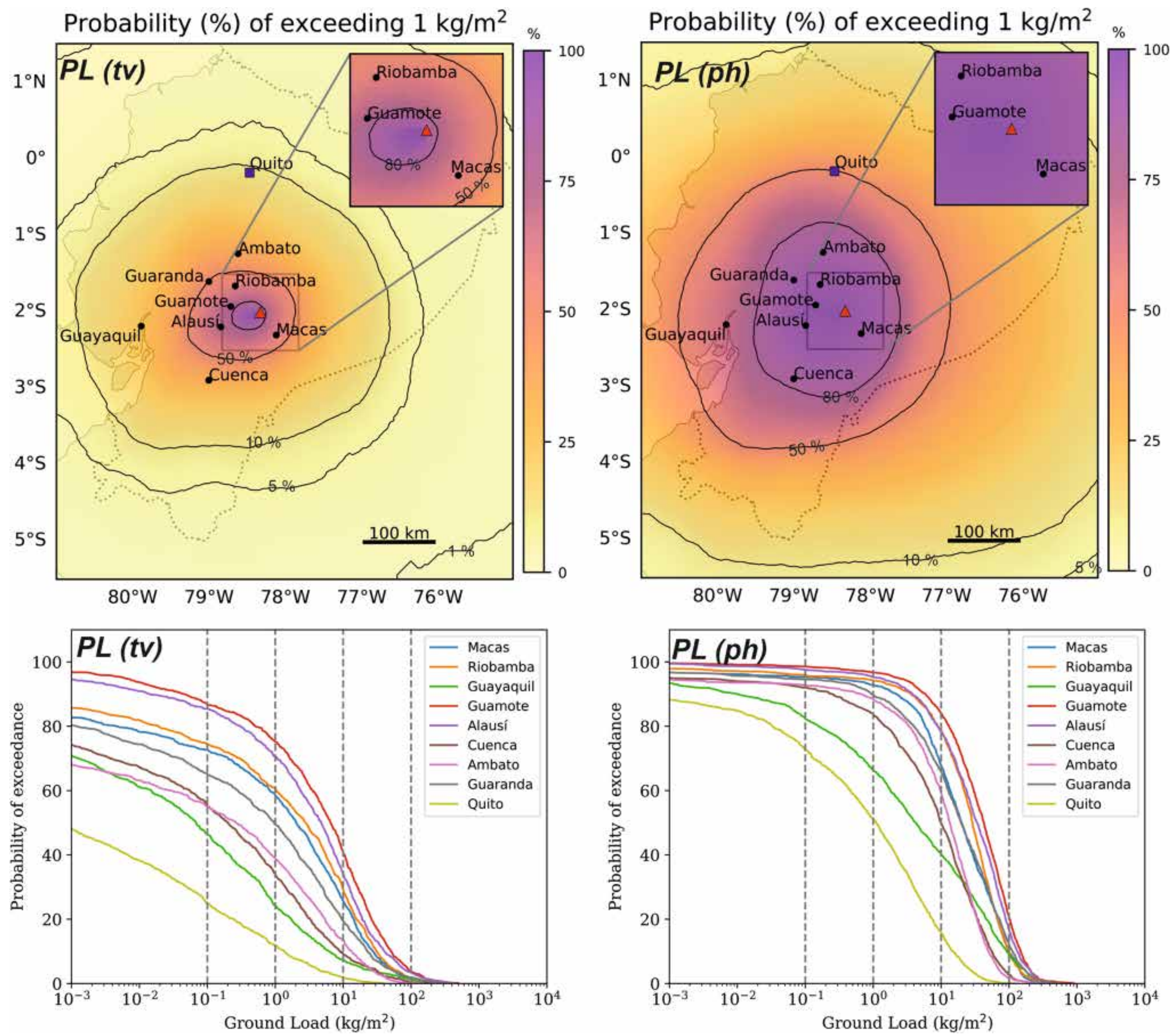

Fig. 9 Upper panels: Sangay tephra fallout hazard maps for the PL scenario for 1 kg/m^2 threshold. Map in the left column is produced by initializing PLUME-MoM with total volume (tv), whereas that in the right column using plume height (ph). Contour lines, where not indicated, follow the progression 1%, 5%, 10%, 50%, and 80%. Lower panels: hazard curves for 9 sites (see Fig. 1) for the PL scenario. Curves in the left column are produced by initializing PLUME-MoM-TSM with total volume (tv), whereas those in the right column by using plume height (ph). Interpolated values at 0.1, 1, 10, and 100 kg/m^2 are reported in Supporting Information 3

at Sangay encloses the town of Guamote, which is the one which would suffer most of tephra accumulation according to our maps/curves. The area impacted by tephra fallout for small eruptions (SAV) is instead more restricted in areas proximal to the volcano excluding Guamote, while our maps/curves indicate a probability of exceeding 1 kg/m^2 of 9–13% even in case of SAV eruptions. In addition, we also note that, in Ordoñez et al. (2011), the towns of Alausí and Riobamba are not enclosed neither within the "moderate" eruption scenario (VS) impact area, while indeed they has been affected, respectively, three times and one time since 2020 by tephra accumulation > 0.1 kg/m^2 (see Table 1).

Differences between the two initialization setups

The differences between the two initialization setups ph and tv are already anticipated from the input parameter distributions (see the "Simulation setting" section) and are more evident for larger magnitude scenarios (i.e., SPL and PL). In the SPL/PL scenarios, and especially in the PL scenario, the

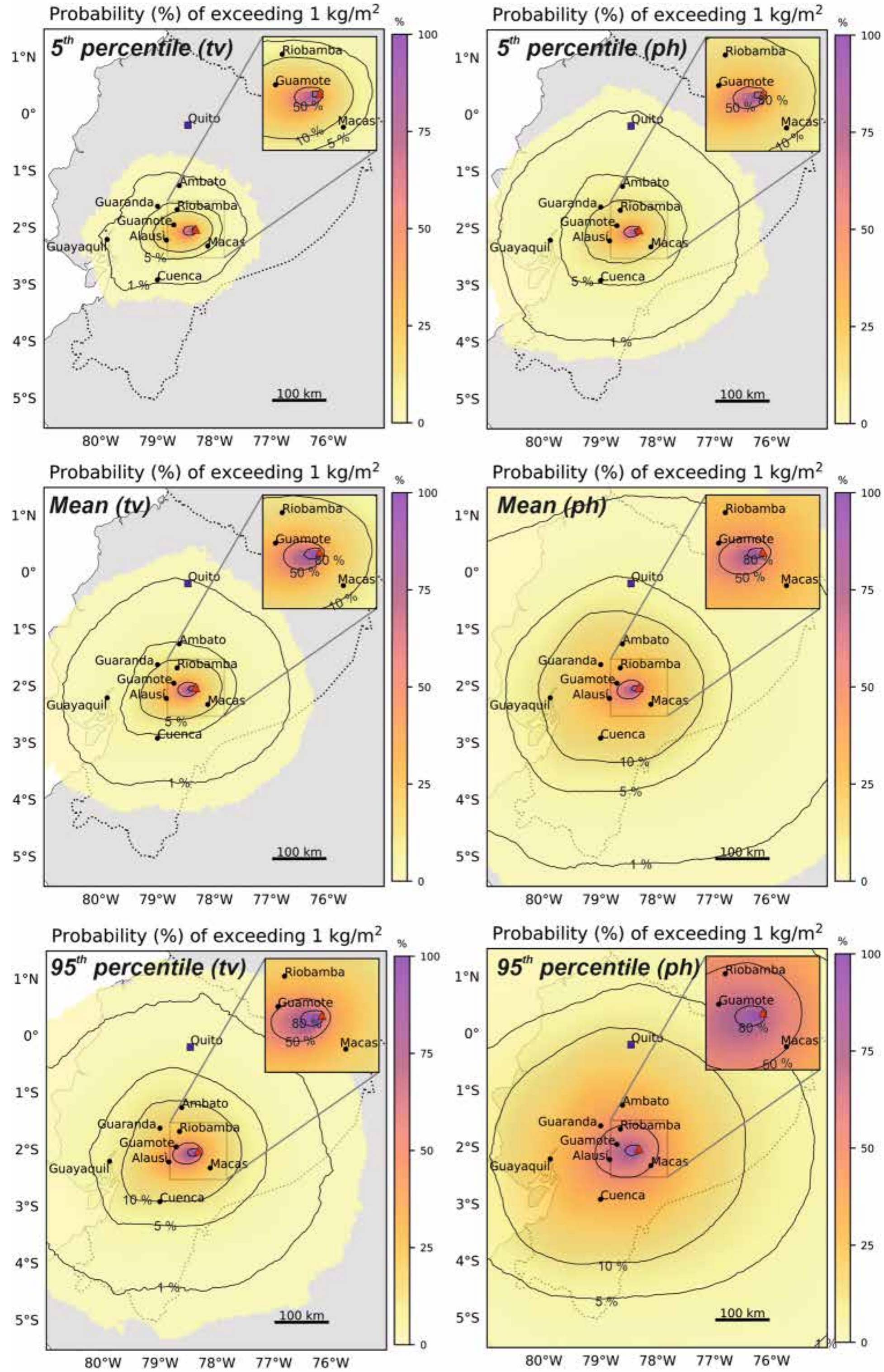

Fig. 10 Sangay tephra fallout hazard maps for the combined SAV, VS, SPL, and PL scenarios for 1 kg/m^2 threshold corresponding to the 5th percentile, the mean, and the 95th percentile. Maps in the left column are produced initializing PLUME-MoM-TSM with total volume (tv), whereas those in the right column using plume height (ph). Contour lines, where not indicated, follow the progression 1%, 5%, 10%, 50%, and 80%

elicited distribution of average plume height is not always consistent to the elicited fallout total volume distribution, and in these scenarios, the ph setup produces a significantly greater fallout hazard than the tv setup (see Fig. 19S from Supporting Information 2).

We remind that when we had to calculate the mass flow rate, we obtained it from the elicited total volume (converted into mass considering an equivalent density of 1000 kg/m^2) and duration and averaged it over the course of the simulated eruption. The high uncertainty in estimating tephra fallout

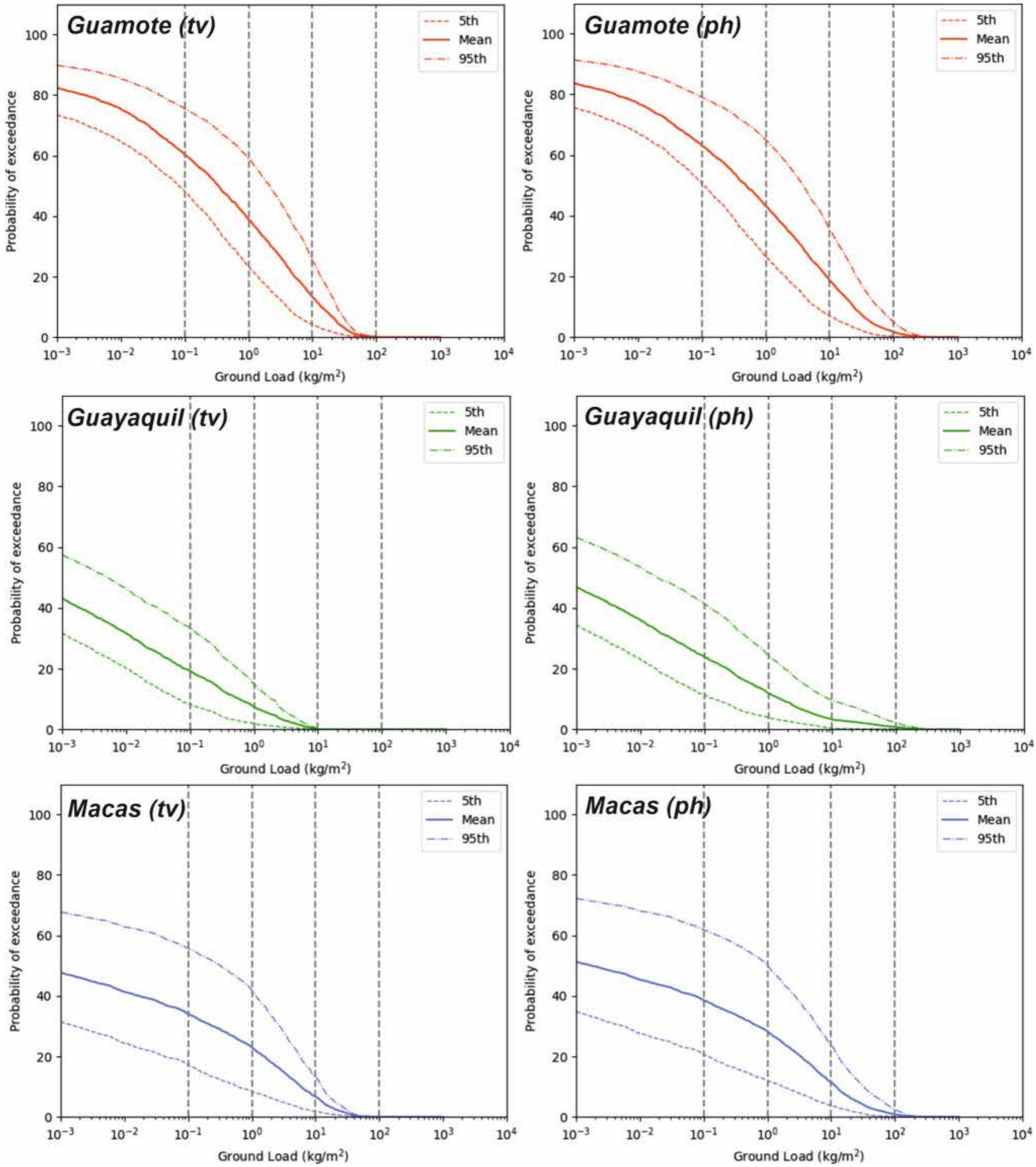

Fig. 11 Hazard curves for 3 sites (Guamote, Guayaquil, and Macas, see Fig. 1) for the combined SAV, VS, SPL, and PL scenarios corresponding to the 5th percentile, the mean, and the 95th percentile. Curves in the left column are produced by initializing PLUME-MoM-TSM with total volume (tv), whereas those in the right column by using plume height (ph). Interpolated values at 0.1, 1, 10, and 100 kg/m^2 are reported in Supporting Information 3

volume/mass, as well as in eruption duration, contributed to the large uncertainty on the mass flow rate, also considering that total volume and duration have been sampled independently in our simulations. Nevertheless, we note that an average plume height that reaches high elevation, not only implies a greater total volume than a lower plume with the

Table 1 Measured ground loads at selected locations from eruptions at Sangay volcano (period June 2020–June 2024)

Measured ground load (kg/m^2) for different eruption type (date)	Town				
	Alausí	*Guamote*	*Guaranda*	*Guayaquil*	*Riobamba*
SAV (8–11/6/20)	0.11	-	-	0.007	-
VS (20/9/20)	0.176–0.187	0.19	-	0.015–0.036	-
VS (5–6/3/21)	2.457	0.041	-	-	-
VS (11/3/21)	-	-	-	-	0.105–0.710
VS (12/4/21)	-	-	0.024–0.046	0.008	-
SAV (12–13/8/22)	0.051	0.026	-	-	-
SAV (4–5/11/22)	0.021	0.128	-	-	-
SAV (18–21/4/23)	0.002	0.207	-	-	-
SAV (21/5/23)	0.02	-	-	-	-
SAV (7/1/24)	-	0.176	-	-	-
SAV (27/1/24)	0.029	0.036	-	-	-
SAV (12/6/24)	-	-	-	0.003	-

same duration, but also allows ash to be transported far from the vent area by the strongest directional winds (see also Fig. 4). This may have enhanced the effect of the uncertainty affecting the plume height on the fallout hazard assessments, if compared to the total volume or the eruption duration.

In particular, we note that the elicitation in Bernard et al. (2024) estimated the total deposit volume, which may underestimate the total erupted volume significantly because of the very fine ash fraction, which does not settle for long periods and can range from a negligible amount to more than 30% of the erupted mass (Rose and Durant 2009). Conversely, the plume height elicitation was considering variable wind conditions, but the wind field in the simulation was sampled independently from the plume height value.

Table 2 Comparison between probability of exceeding different ground load (GL) thresholds (0.1 and 1 kg/m^2) and the percentage of eruptive pulses which have produced ground loads larger than the same thresholds at five sites. The range of some exceeding probabilities takes into account the differences between the two initialization setups (tv and ph) for the single scenarios (SAV and VS, see Supporting Information 3). Cells with "-" indicate that for this site/eruption type, no eruption had a GL ≥ the considered threshold

Town	Eruption type	Initialization	Modeled probability of exceeding 0.1 kg/m^2	Binomial probability of the observed eruptions with GL > 0.1 kg/m^2	Modeled probability of exceeding 1 kg/m^2	Binomial probability of the observed eruptions with GL > 1 kg/m^2
Alausí	SAV	tv	20%	34%	3%	79%
		ph	32%	17%	9%	47%
	VS	tv	44%	37%	16%	38%
		ph	46%	37%	18%	40%
Guamote	SAV	tv	25%	20%	5%	69%
		ph	38%	28%	13%	34%
	VS	tv	51%	24%	24%	33%
		ph	48%	27%	21%	39%
Guaranda	SAV	tv	4%	74%	0%	98%
		ph	7%	56%	0%	98%
	VS	tv	14%	54%	2%	92%
		ph	14%	55%	3%	88%
Guayaquil	SAV	tv	0%	97%	0%	99%
		ph	3%	81%	0%	99%
	VS	tv	6%	77%	1%	98%
		ph	6%	78%	0%	99%
Riobamba	SAV	tv	7%	58%	1%	94%
		ph	11%	41%	2%	88%
	VS	tv	21%	41%	7%	74%
		ph	21%	41%	8%	71%

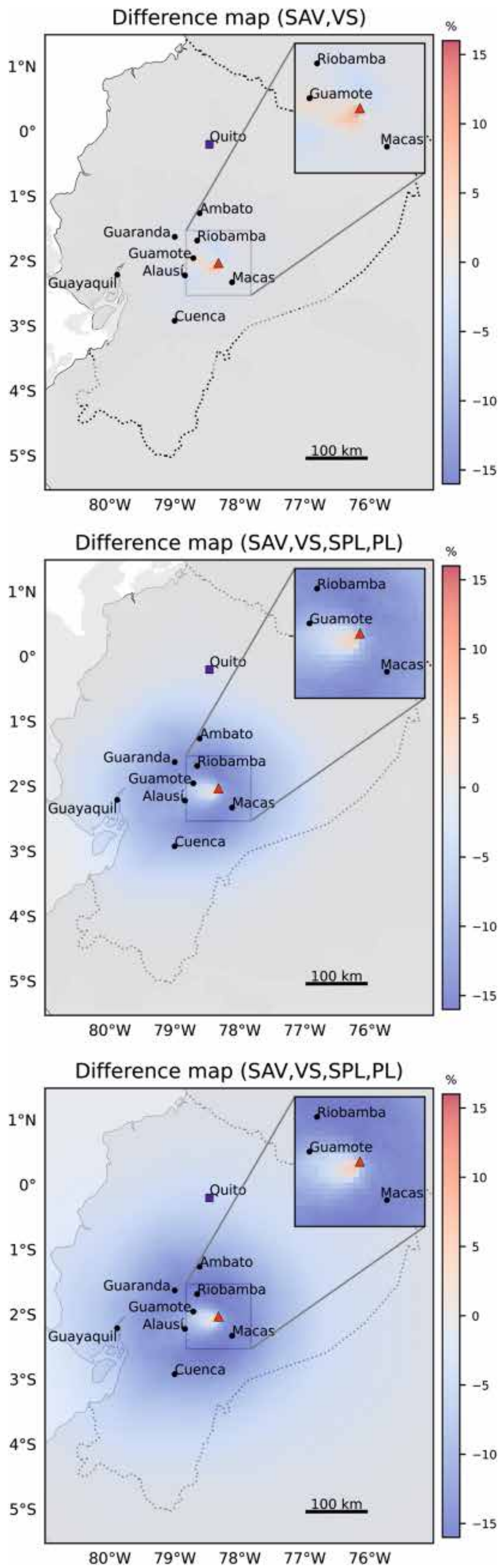

Fig. 12 Difference maps obtained as a difference between the mean maps of the two initialization approaches (tv and ph) for, respectively, SAV-VS, SAV-VS-SPL, and SAV-VS-SPL-PL maps (see titles)

Consequently, the association of high plumes and strong winds may have produced an over-estimation of the erupted volume in the second approach.

To quantify these differences, we have produced (Fig. 12) difference maps between the combined mean maps of the two initialization setups (SAV-VS, SAV-VS-SPL, and SAV-VS-SPL-PL). In Fig. 12, maps initialized with ph are subtracted from the maps initialized with tv: this implies that negative values are those where ph maps have higher mean probability and vice versa. In Fig. 12, we observe that tv maps are characterized by higher hazard values in areas proximal (< 25 km to the W) with respect to Sangay location (with values never exceeding +5% in Fig. 12), while ph maps imply higher probabilities on medial-distal areas (values up to 16% more than mfr maps in Fig. 12).

Despite these differences, there is not a strong physical evidence for preferring one type of initialization over the other, because all the ESPs are significantly uncertain. However, we note that during the elicitation, the experts provided a numerical value (in a scale from 1 to 10) expressing their own confidence in estimating the considered ESPs, and in this regard, average plume height attained a slightly higher confidence with respect to total volume and duration (Bernard et al. 2024).

While we are not suggesting a preference for an initialization over the other, we stress that the choice made might have implications for vulnerability/risk assessment studies. For example, considering the SAV-VS-SPL maps, the probability (% - [5^{th}-*Mean*−95^{th}]) of having ≥ 1 kg/m^2 threshold (roughly corresponding to 1 mm of ash accumulation, sufficient for airport closure) for the site of Guayaquil is, respectively, [0.6-*1.3*−2.3] for the tv initialization and [1.8-*7.4*−15.0] for the ph initialization (see Fig. 8 and Supporting Information 3). Similarly, the probability (% - [5^{th}-*Mean*−95^{th}]) of having ≥ 10 kg/m^2 threshold (roughly corresponding to 10 mm of ash accumulation, sufficient for minor structural damages to edifices) for the site of Guamote is, respectively, [1.4-*3.8*−7.0] for the tv initialization and [4.1-*13.3*−25.4] for the ph initialization (see Fig. 8 and Supporting Information 3). In both examples, the differences between the two model initializations is 3–5 times higher for the ph.

By looking at Figs. 5 and 6 (and Fig. 19S from Supporting Information 2), we finally observe that, for SAV/VS initialized with tv and SPL/PL initialized with ph, our filtering approach rejected a larger number of ESPs. We have therefore produced a “mixed” set of maps, in which we applied the same procedure of the “Type of outputs” section (Eq. (4)), but combining only the maps with the ph initialization for SAV and VS, and the maps with the tv initialization for SPL/PL. Results (maps and hazard curves) are displayed in Figures 26S-31S from Supporting Information 2.

Concluding remarks

This study provides a new tephra fallout hazard assessment for Sangay volcano through the production of probabilistic hazard maps and curves. These products have been developed using the coupled PLUME-MoM/HYSPLIT models with inputs from a stochastic sampling of atmospheric conditions and eruptive source parameters. The model itself has been initialized with either total volume and average plume height, producing two different types of maps. Four different scenarios (corresponding to eruptive pulses, Bernard et al. 2024) have been considered, and maps for each scenario have been produced for four different ground load thresholds (0.1, 1, 10, and 100 kg/m^2). Hazard curves (representing exceedance probabilities) have also been produced in nine sites located both in the surroundings and at more distal locations from Sangay volcano. Maps for single eruptive scenarios have been combined according to the probability of having at least one such scenario over the next 100 years. Such probabilities (along with the eruptive source parameters for each scenario) and their uncertainties have been quantified through an expert elicitation session described in the companion paper by Bernard et al. (2024). Combined maps and curves take into account the uncertainty in probability of occurrences of different eruptive pulses in the next 100 years and are therefore presented, for each combination setup, as mean maps and 5th/95th percentile maps, the latter two representing the uncertainty bounds.

Main results include:

- Maps and curves for both single and combined scenarios indicate that the highest tephra fallout hazard is toward the W of Sangay volcano, consistently with observed volcanic activity and dominant wind directions. The town of Guamote (43 km W of Sangay) is the site, among the investigated ones, with the highest hazard, as it could be potentially affected by significant tephra accumulation (1 kg/m^2) with probabilities up to 21–24% even for a moderate-scale eruption (Violent Strombolian).
- For combined scenarios, maps and curves were produced by integrating, respectively, (i) the three historically observed eruptive pulses (Strong Ash Venting, Violent Strombolian, and sub-Plinian), (ii) the previous three and a larger Plinian event, and (iii) the two smallest observed pulses (Strong Ash Venting and Violent Strombolian. Average differences between combinations (i) and (ii) at the nine locations with hazard curves are between ~6 and ~9% for all the considered ground load thresholds and the two initialization setups. However, average differences up to 28–40% could be observed for few sites and ground loads.
- Differences between initialization setups have been quantified for the mean maps and indicate that maps with total volume initialization produce higher hazards (+5% maximum) for locations proximal to vent area (i.e., < 25 km to the W of Sangay) but lower hazards (−15% maximum) for medial-distal locations; possible reasons for this effect are the assumption of an erupted volume equal to the deposited volume and the assumed independency of plume height and wind conditions.

All the outcomes summarized above clearly demonstrate the numerous sources of uncertainty that affect hazard maps and curves, related to the eruptive source parameters and atmospheric conditions (when producing maps for single scenarios), the type of model initialization (when adopting different source parameters), and the probability of occurrence of different scenarios (when combining maps from multiple scenarios). Nevertheless, a first comparison of the recent activity of Sangay is consistent with our hazard product. We believe that the set of maps and curves produced, obtained under different assumptions and with the associated uncertainty, can represent a valuable information for authorities and decision-makers aimed at mitigating the tephra fallout hazard at Sangay volcano.

Supplementary Information The online version contains supplementary material available at https://doi.org/10.1007/s00445-025-01794-4.

Acknowledgements We thank Maurizio Mulas from the ESPOL for kindly providing samples from Guayaquil and Rúben Chérrez and Pablo Ruiz from the ROVE for kindly providing samples from Guaranda and Riobamba. We also thank Marjorie Encalada and Edwin Telenchana for the help in collecting some field data used in this study. We finally thank Silvia Massaro for the editorial handling and two anonymous reviewers for insightful comments that improved the quality of the manuscript.

Author contribution Conceptualization: All; methodology: AT, FP, AB, BB, MdMV, AA, AN; formal analysis and investigation: AT, FP, AB; writing—original draft preparation: AT, FP, AB; writing—review and editing: All; resources: AT, FP, AB, BB.

Funding AT was partially funded by CONVENZIONE ATTUATIVA PER IL POTENZIAMENTO DELLE ATTIVITA' DI SERVIZIO A.Q. DPC-INGV 2022-2025. AA was supported by the ANID Iniciativa Milenio-ICN2021_038 "Millenium Institute on Volcanic Risk Research - Ckelar Volcanoes". AT, AA, PS, NA and OR acknowledge the support received from the Agence Nationale de la Recherche of the French government through the program ''Investissements d'Avenir'' (16-IDEX-0001 CAP 20-25). This work was partially supported by the project "Pianeta Dinamico (Dynamic Planet)-Working Earth"–WUNDERVUL "Toward a Wider Understanding of Vulcano", funded by the Italian Ministry of Education, University and Research.

Declarations

Competing interests The authors declare that they have no competing interests. AT, AB, and AA are editor for the Special Issue "Uncertainty Quantification in Volcanology: Observations, Numerical Modelling and Hazard/Risk Assessment".

References

Annen C, Wagner JJ (2003) The impact of volcanic eruptions during the 1990s. Nat Hazards Rev 44(4):1694–175. https://doi.org/10.1061/(ASCE)1527-6988(2003)4:4(169)

Aravena A, Bevilacqua A, Neri A, Gabellini P, Ferrés D, Escobar D, Aiuppa A, Cioni R (2023) Scenario-based probabilistic hazard assessment for explosive events at the San Salvador Volcanic complex, El Salvador. J Volcanol Geotherm Res 438:107809. https://doi.org/10.1016/j.jvolgeores.2023.107809

Aspinall WP (2006) Structured elicitation of expert judgment for probabilistic hazard and risk assessment in volcanic eruptions. Statistics in Volcanology 1:15–30

Aspinall WP, Cooke RM (2013) Quantifying scientific uncertainty from expert judgment elicitation. In: Rougier J, Sparks RSJ, Hill LJ (eds) Risk and uncertainty assessment for natural hazards. Cambridge University Press, New York, pp 64–99. https://doi.org/10.1017/CBO9781139047562

Barker SJ, Van Eaton AR, Mastin LG, Wilson CJ, Thompson MA, Wilson TM, Davis C, Renwick JA (2019) Modeling ash dispersal from future eruptions of Taupo supervolcano. Geochem Geophys Geosystems 20(7):3375–3401. https://doi.org/10.1029/2018GC008152

Barsotti S, Di Rienzo DI, Thordarson T, Björnsson BB, Karlsdóttir S (2018) Assessing impact to infrastructures due to tephra fallout from Öræfajökull volcano (Iceland) by using a scenario-based approach and a numerical model. Front Earth Sci 6:196. https://doi.org/10.3389/feart.2018.00196

Barsotti S, Andronico D, Neri A, Del Carlo P, Baxter PJ, Aspinall WP, Hincks T (2010) Quantitative assessment of volcanic ash hazards for health and infrastructure at Mt. Etna (Italy) by numerical simulation J Volcanol Geotherm Res 192(1-2), 85-96. https://doi.org/10.1016/j.jvolgeores.2010.02.011

Baxter, P. J., and Horwell, C. J. (2015). Impacts of eruptions on human health. In H. Sigurdsson, B. F. Houghton, S. R. McNutt, H. Rymer, and J. Stix (Eds.), The encyclopedia of volcanoes. Elsevier, pp. 1035–1047. https://doi.org/10.1016/B978-0-12-385938-9.00060-2

Bebbington MS, Cronin SJ, Chapman I, Turner MB (2008) Quantifying volcanic ash fall hazard to electricity infrastructure. Journal of Volcanology and Geothermal Research 177(4):1055–1062. https://doi.org/10.1016/j.jvolgeores.2008.07.023

Bernard B, Samaniego P, Mastin L, Hernandez S, Pino G, Kibler J, Encalada M, Hidalgo S, Vizuete N (2022) Forecasting and communicating the dispersion and fallout of ash during volcanic eruptions: lessons from the September 20, 2020 eruptive pulse at Sangay volcano, Ecuador. Front. Earth Sci 10. https://doi.org/10.3389/feart.2022.912835.

Bernard B, Tadini A, Samaniego PBevilacqua A, Vasconez FJ, Aravena A, de' Michieli Vitturi M, Hidalgo S (2024) Developing hazard scenarios from monitoring data, historical chronicles and expert elicitation: case study of Sangay volcano, Ecuador. https://doi.org/10.21203/rs.3.rs-3764842/v1

Bevilacqua A, Isaia R, Neri A, Vitale S, Aspinall WP, Bisson M, Flandoli F, Baxter PJ, Bertagnini A, Esposti Ongaro T, Iannuzzi E, Pistolesi M, Rosi M (2015) Quantifying volcanic hazard at Campi Flegrei caldera (Italy) with uncertainty assessment: I. Vent opening maps. J Geophys Res Solid Earth 120:2309–2329. https://doi.org/10.1002/2014JB011775

Bevilacqua A, Flandoli F, Neri A, Isaia R, Vitale S (2016) Temporal models for the episodic volcanism of Campi Flegrei caldera (Italy) with uncertainty quantification. J Geophys Res Solid Earth 121:7821–7845. https://doi.org/10.1002/2016JB013171

Bevilacqua A, Bursik M, Patra A, Pitman EB, Yang Q, Sangani R, Kobs- Nawotniak S (2018) Late Quaternary eruption record and probability of future volcanic eruptions in the Long Valley volcanic region (CA, USA). J Geophys Res Solid Earth 123(7):5466–5494. https://doi.org/10.1029/2018JB015644

Bevilacqua A, Aravena A, Neri A, Gutiérrez E, Escobar D, Schliz M, Aiuppa A, Cioni R (2021) Thematic vent opening probability maps and hazard assessment of small-scale pyroclastic density currents in the San Salvador volcanic complex (El Salvador) and Nejapa-Chiltepe volcanic complex (Nicaragua). Nat Hazards Earth Syst Sci 21:1639–1665. https://doi.org/10.5194/nhess-21-1639-2021

Bevilacqua A, Aravena A, Aspinall W, Costa A, Mahony S, Neri A, Sparks R, Hill B (2022) Assessing minimum pyroclastic density current mass to impact critical infrastructures: example from Aso caldera (Japan). Nat Hazards Earth Syst Sci 22(10):3329–3348. https://doi.org/10.5194/nhess-22-3329-2022

Biass S, Bonadonna C (2011) A quantitative uncertainty assessment of eruptive parameters derived from tephra deposits: the example of two large eruptions of Cotopaxi volcano Ecuador. Nat Hazards Earth Syst Sci 73(1):73–90. https://doi.org/10.1007/s00445-010-0404-5

Biass S, Bonadonna C (2013) A fast GIS-based risk assessment for tephra fallout: the example of Cotopaxi volcano Ecuador. Nat Hazards 65(1):477–495. https://doi.org/10.1007/s11069-012-0378-z

Blong RJ (1996) Volcanic hazards risk assessment. In R. Scarpa, & R. I. Tilling (Eds.), Monitoring and mitigation of volcano hazards. Berlin, Springer, pp. 675–698. https://doi.org/10.1007/978-3-642-80087-0_20.

Bonadonna C (2006) Probabilistic modelling of tephra dispersion. In: Mader HM, Coles SG, Connor CB, Connor LJ (eds) Statistics in volcanology. Geological Society, London, pp 243–259

Bonasia R, Capra L, Costa A, Macedonio G, Saucedo R (2011) Tephra fallout hazard assessment for a Plinian eruption scenario at Volcán de Colima (Mexico). J Volcanol Geotherm Res 203(1–2):12–22. https://doi.org/10.1016/j.jvolgeores.2011.03.006

Bonasia R, Scaini C, Capra L, Nathenson M, Siebe C, Arana-Salinas L, Folch A (2014) Long-range hazard assessment of volcanic ash dispersal for a Plinian eruptive scenario at Popocatépetl volcano (Mexico): implications for civil aviation safety. Bull Volcanol 76:1–16. https://doi.org/10.1007/s00445-013-0789-z

Constantinescu R, White JT, Connor CB, Hopulele-Gligor A, Charbonnier S, Thouret JC, Lindsay JM, Bertin D (2022) Uncertainty quantification of eruption source parameters estimated from tephra fall deposits. Geophys. Res. Lett 49(6), e2021GL097425. https://doi.org/10.1029/2021GL097425

Cooke, R. M. (1991). Experts in uncertainty: Opinion and subjective probability in science. https://doi.org/10.1093/oso/9780195064650.001.0001

de' Michieli Vitturi M, Pardini F (2021) PLUME-MoM-TSM 1.0. 0: a volcanic column and umbrella cloud spreading model. Geosci Model Dev 14(3):1345–1377. https://doi.org/10.5194/gmd-14-1345-2021

de' Michieli Vitturi M, Engwell SL, Neri A, Barsotti, S. (2016). Uncertainty quantification and sensitivity analysis of volcanic columns models: results from the integral model PLUME-MoM. J Volcanol Geotherm Res 326:77-91.https://doi.org/10.1016/j.jvolgeores.2016.03.014

de' Michieli Vitturi M, Bevilacqua A, Tadini A, Neri A (2024) ELICIPY 1.0: a Python online tool for expert elicitation. SoftwareX 25. https://doi.org/10.1016/j.softx.2024.101641

Flandoli F, Giorgi E, Aspinall WP, Neri A (2011) Comparison of a new expert elicitation model with the classical model, equal weights and single experts, using a cross-validation technique. Reliab Eng. Syst. Saf. 96:1292–1310. https://doi.org/10.1016/j.ress.2011.05.012

Hersbach H, Bell B, Berrisford P, Hirahara S, Horányi A, Muñoz-Sabater J, Nicolas J, Peubey C, Radu R, Schepers D, Simmons A, Soci C, Abdalla S, Abellan X, Balsamo G, Bechtold P, Biavati G, Bidlot J, Bonavita M, De Chiara G, Dahlgren P, Dee D, Diamantakis M, Dragani R, Flemming J, Forbes R, Fuentes M, Geer A, Haimberger L, Healy S, Hogan RJ, Hólm E, Janisková M, Keeley S, Laloyaux P, Lopez P, Lupu C, Radnoti G, de Rosnay P, Rozum I, Vamborg F, Villaume S, Thépaut JN (2020) The ERA5 global reanalysis. Quarterly Journal of the Royal Meteorological Society 146(730):1999–2049. https://doi.org/10.1002/qj.3803

Hidalgo S, Vasconez FJ, Battaglia J, Bernard B, Espín P, Valade S, Naranjo M-F, Campion, R., Salgado, J., Córdova, M., Almeida, M., Hernández, S., Pino, G., Gaunt, E., Bell, A., Mothes, P., and Ruiz, M. (2022). Sangay volcano (Ecuador): the opening of two new vents, a drumbeat seismic sequence and a new lava flow in late 2021. Volcanica 5(2):2. https://doi.org/10.30909/vol.05.02.295311.

Hurst T, Smith W (2004) A Monte Carlo methodology for modelling ashfall hazards. J Volcanol Geotherm Res 138(3–4):393–403. https://doi.org/10.1016/j.jvolgeores.2004.08.001

Jenkins S, McAneney J, Magill C, Blong R (2012) Regional ash fall hazard II: Asia-Pacific modelling results and implications. Bull Volcanol 74:1713–1727. https://doi.org/10.1007/s00445-012-0628-7

Jenkins SF, Wilson TM, Magill CR, Miller V, Stewart C, Marzocchi W, Boulton M (2015) Volcanic ash fall hazard and risk: technical background paper for the UNISDR 2015 global assessment report on disaster risk reduction (Global Volcano Model and IAVCEI). www.preventionweb.net/english/hyogo/gar

Ligot N, Viera W, Peñaherrera D, Bernard B, Bogaert P, Delmelle P (2024) A quantitative assessment of crop vulnerability to tephra hazard at Tungurahua volcano, Ecuador: understanding the effect of volcanic and biological factors. Bull Volcanol 86(4):28. https://doi.org/10.1007/s00445-024-01710-2

Macedonio G, Costa A (2012) Brief communication “rain effect on the load of tephra deposits.” Nat Hazards Earth Syst Sci 12(4):1229–1233. https://doi.org/10.5194/nhess-12-1229-2012

Macedonio G, Costa A, Scollo S, Neri A (2016) Effects of eruption source parameter variation and meteorological dataset on tephra fallout hazard assessment: example from Vesuvius (Italy). J Appl Volcan 5(1):1. https://doi.org/10.1186/s13617-016-0045-2

Madankan R, Pouget S, Singla P, Bursik MI, Dehn J, Jones M, Patra A, Pavolonis M, Pitman EB, Singh T, Webley P (2014) Computation of probabilistic hazard maps and source parameter estimation for volcanic ash transport and dispersion. J Comput Phys 271:39–59. https://doi.org/10.1016/j.jcp.2013.11.032

Magill C, Wilson T, Okada T (2013) Observations of tephra fall impacts from the 2011 Shinmoedake eruption, Japan. Earth, Planets and Space 65:677–698. https://doi.org/10.5047/eps.2013.05.010

Mastin LG, Guffanti M, Servranckx R, Webley P, Barsotti S, Dean K, Durant A, Ewert JW, Neri A, Rose WI, Schneider D, Siebert L, Stunder B, Swanson G, Tupper A, Volentik A, Waythomas CF (2009) A multidisciplinary effort to assign realistic source parameters to models of volcanic ash-cloud transport and dispersion during eruptions. J Volcanol Geotherm Res 186(1–2):10–21. https://doi.org/10.1016/j.jvolgeores.2009.01.008

Mastin LG, Van Eaton AR, Schneider D, Denlinger RP (2017) Ongoing efforts to make ash-cloud model forecasts more accurate. NATO Science and Technology Organization, Brussels, Belgium

Michaud-Dubuy A, Carazzo G, Kaminski E (2021) Volcanic hazard assessment for tephra fallout in Martinique. J Appl Volcan 10:1–20. https://doi.org/10.1186/s13617-021-00106-7

Monzier M, Robin C, Samaniego P, Hall ML, Cotten J, Mothes P, Arnaud N (1999) Sangay volcano, Ecuador: structural development, present activity and petrology. J Volcanol Geotherm Res 90(1–2):49–79. https://doi.org/10.1016/S0377-0273(99)00021-9

Moran-Zuloaga D, Merchan-Merchan W, Rodriguez-Caballero E, Mulas M, Hernick P (2023) Long-range transport and microscopy analysis of Sangay volcanic ashes in Ecuador. Air Qual Atmos Hlth. https://doi.org/10.1007/s11869-023-01434-w

Neri A, Aspinall WP, Cioni R, Bertagnini A, Baxter PJ, Zuccaro G, Andronico D, Barsotti S, Cole PD, Esposti Ongaro T (2008) Developing an event tree for probabilistic hazard and risk assessment at Vesuvius. J Volcanol Geotherm Res 178:397–415. https://doi.org/10.1016/j.jvolgeores.2008.05.014

Neri A, Bevilacqua A, Esposti Ongaro T, Isaia R, Aspinall WP, Bisson M, Flandoli F, Baxter PJ, Bertagnini A, Iannuzzi E (2015) Quantifying volcanic hazard at Campi Flegrei caldera (Italy) with uncertainty assessment: II. Pyroclastic density current invasion maps. J Geophys Res Solid Earth 120:2330–2349. https://doi.org/10.1002/2014JB011776

Ordoñez J, Vallejo SV, Bustillos J, Hall M, Andrade D, Hidalgo S, Samaniego P (2011) Volcán Sangay, peligros volcánicos potenciales. IG-EPN/IRD. Escala 1(100):000

Pardini F, Corradini S, Costa A, Esposti Ongaro T, Merucci L, Neri A, Stelitano D, de' Michieli Vitturi M (2020) Ensemble-based data assimilation of volcanic ash clouds from satellite observations: application to the 24 December 2018 Mt. Etna explosive eruption. Atmosphere 11(4): 359.https://doi.org/10.3390/atmos11040359

Rose WI, Durant AJ (2009) Fine ash content of explosive eruptions. J Volcanol Geotherm Res 186(1–2):32–39. https://doi.org/10.1016/j.jvolgeores.2009.01.010

Sandri L, Costa A, Selva J, Tonini R, Macedonio G, Folch A, Sulpizio R (2016) Beyond eruptive scenarios: assessing tephra fallout hazard from Neapolitan volcanoes. Sci Rep 6(1):1–13. https://doi.org/10.1038/srep24271

Stefanescu ER, Patra AK, Bursik MI, Madankan R, Pouget S, Jones M, Singla P, Singh T, Pitman EB, Pavolonis M, Morton D, Webley P, Dehn J (2014) Temporal, probabilistic mapping of ash clouds using wind field stochastic variability and uncertain eruption source parameters: example of the 14 April 2010 Eyjafjallajökull eruption. J Adv Model Earth Syst 6(4):1173–1184. https://doi.org/10.1002/2014MS000332

Stein AF, Draxler RR, Rolph GD, Stunder BJB, Cohen MD, Ngan F (2015) NOAA's HYSPLIT atmospheric transport and dispersion modeling system. Bull Am Meterol Soc 96(12):2059–2077. https://doi.org/10.1175/BAMS-D-14-00110.1

Tadini A, Bisson M, Neri A, Cioni R, Bevilacqua A, Aspinall WP (2017a) Assessing future vent opening locations at the Somma-Vesuvio volcanic complex: 1. A new information geodatabase with uncertainty characterizations. J Geophys Res Solid Earth 122:4336–4356. https://doi.org/10.1002/2016JB013858

Tadini A, Bevilacqua A, Neri A, Cioni R, Aspinall WP, Bisson M, Isaia R, Mazzarini F, Valentine GAV, Vitale S, Baxter PJ, Bertagnini Acerminara M, de' Michieli Vitturi M, Di Roberto A, Engwell SLEsposti Ongaro T, Flandoli F, Pistolesi M (2017b) Assessing future vent opening locations at the Somma-Vesuvio volcanic complex: 2. Probability maps of the caldera for a future Plinian/sub-Plinian event with uncertainty quantification. J. Geophys. Res. Solid Earth 122:4357–4376.https://doi.org/10.1002/2016JB013860

Tadini A, Roche O, Samaniego P, Guillin A, Azzaoui N, Gouhier M, de' Michieli Vitturi, M, Pardini F, Eychenne J, Bernard B, Hidalgo S, Le Pennec JL (2020) Quantifying the uncertainty of a coupled plume and tephra dispersal model: PLUME-MOM/HYSPLIT simulations applied to Andean volcanoes. J Geophys Res Solid Earth 125(2). https://doi.org/10.1029/2019JB018390

Tadini A, Roche O, Samaniego P, Azzaoui N, Bevilacqua A, Guillin A, Gouhier Mbernard B, Aspinall W, Hidalgo S, Eychenne J, de' Michieli Vitturi M, Neri A, Cioni R, Pistolesi M, Gaunt E, Vallejo S, Encalada M, Yepes H, Proaño A, Pique M (2021) Eruption type probability and eruption source parameters at Cotopaxi and Guagua Pichincha volcanoes (Ecuador) with uncertainty quantification. Bull Volcanol 83(35). https://doi.org/10.1007/s00445-021-01458-z.

Tadini A, Azzaoui N, Roche O, Samaniego P, Bernard B, Bevilacqua A, Hidalgo S, Guillin A, Gouhier M (2022) Tephra fallout probabilistic hazard maps for Cotopaxi and Guagua Pichincha volcanoes (Ecuador) with uncertainty quantification. J Geophys Res Solid Earth 127:e2021JB022780. https://doi.org/10.1029/2021JB022780.

Titos M, Martínez Montesinos B, Barsotti S, Sandri L, Folch A, Mingari L, Macedonio G, Costa A (2022) Long-term hazard assessment of explosive eruptions at Jan Mayen (Norway) and implications for air traffic in the North Atlantic. Nat Hazards Earth Syst Sci 22(1):139–163. https://doi.org/10.5194/nhess-22-139-2022

Vasconez FJ, Hidalgo S, Battaglia J, Hernandez S, Bernard B, Coppola D, Valade S, Ramón P, Arellano S, Liorzou C, Almeida M, Ortíz M, Córdova J, Vásconez Müller A (2022) Linking ground-based data and satellite monitoring to understand the last two decades of eruptive activity at Sangay volcano, Ecuador. Bull Volcanol 84:49. https://doi.org/10.1007/s00445-022-01560-w

Vázquez R, Bonasia R, Folch A, Arce JL, Macías JL (2019) Tephra fallout hazard assessment at Tacaná volcano (Mexico). J South Am Earth Sci 91:253–259. https://doi.org/10.1016/j.jsames.2019.02.013

Wilson TM, Stewart C, Sword-Daniels V, Leonard GS, Johnston DM, Cole JW et al (2012) Volcanic ash impacts on critical infrastructure. Phys Chem Earth Parts A/B/C 45:5–23. https://doi.org/10.1016/j.pce.2011.06.006

Woodhouse MJ, Hogg AJ, Phillips JC, Rougier JC (2015) Uncertainty analysis of a model of wind-blown volcanic plumes. Bull Volcanol 77:83. https://doi.org/10.1007/s00445-015-0959-2

Yang Q, Pitman EB, Spiller E, Bursik M, Bevilacqua A (2020) Novel statistical emulator construction for volcanic ash transport model Ash3d with physically motivated measures. Proc R Soc A 476:20200161. https://doi.org/10.1098/rspa.2020.0161

Yang Q, Jenkins SF (2023) Two sources of uncertainty in estimating tephra volumes from isopachs: perspectives and quantification. Bull Volcanol 85(8):44. https://doi.org/10.1007/s00445-023-01652-1.